CHAPTER

6

Ideal Flow

OUTLINE

CHAPTER OBJECTIVES

- To describe the formulation and limitations of ideal flow theory.
- To illustrate the use of the stream function and the velocity potential in two-dimensional, axisymmetric, and three-dimensional flows.
- To derive and present classical ideal flow results for flows past simple objects.

© 2012 Elsevier Inc. All rights reserved.

6.1. RELEVANCE OF IRROTATIONAL CONSTANT-DENSITY FLOW THEORY

When a constant-density fluid flows without rotation, and pressure is measured relative to its local hydrostatic value (see Section 4.9), the equations of fluid motion in an inertial frame of reference, (4.7) and (4.38), simplify to:

$$\nabla \cdot \mathbf{u} = 0 \text{ and } \rho(D\mathbf{u}/Dt) = -\nabla p, \qquad (4.10, 6.1)$$

even though the fluid's viscosity μ may be nonzero. These are the equations of *ideal* flow. They are useful for developing a first-cut understanding of nearly any macroscopic fluid flow, and are directly applicable to low-Mach-number irrotational flows of homogeneous fluids away from solid boundaries. Ideal flow theory has abundant applications in the exterior aero- and hydrodynamics of moderate- to large-scale objects at nontrivial subsonic speeds. Here, moderate size (L) and nontrivial speed (U) are determined jointly by the requirement that the Reynolds number, $\mathrm{Re} = \rho UL/\mu$ (4.103), be large enough (typically $\mathrm{Re} \sim 10^3$ or greater) so that the combined influence of fluid viscosity and fluid element rotation is confined to thin layers on solid surfaces, commonly known as *boundary layers*.

The conditions necessary for the application of ideal flow theory are commonly present on the upstream side of many ordinary objects, and may even persist to the downstream side of some. Ideal flow analysis can predict fluid velocity away from solid surfaces, surface-normal pressure forces (when the boundary layer is thin and attached), acoustic streamlines, flow patterns that minimize form drag, and unsteady-flow, fluid-inertia effects. Ideal flow theory does not predict viscous effects like skin friction or energy dissipation, so it is not directly applicable to interior flows in pipes and ducts, to boundary layer flows, or to any rotational flow region. This final specification excludes low-Re flows and regions of turbulence.

Because (6.1) involves only first-order spatial derivatives, ideal flows only satisfy the no-through-flow boundary condition on solid surfaces. The no-slip boundary condition is not applied in ideal flows, so nonzero tangential velocity at a solid surface may exist

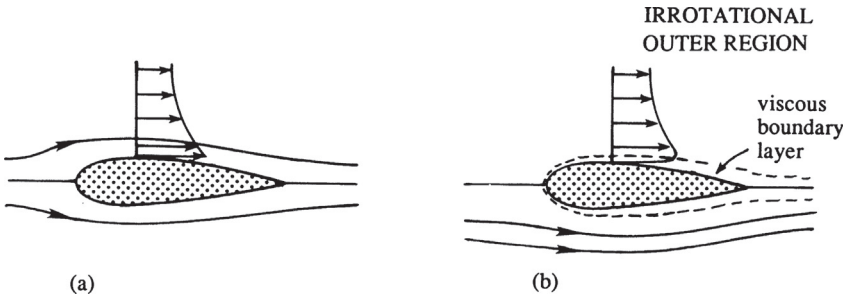

FIGURE 6.1 Comparison of a completely irrotational constant-density (ideal) flow (a) and a high Reynolds number flow (b). In both cases the no-through-flow boundary condition is applied. However, the ideal flow is effectively inviscid and the fluid velocity is tangent to and nonzero on the body surface. The high-Re flow includes thin boundary layers where fluid rotation and viscous effects are prevalent, and the non-slip boundary condition is enforced, but the velocity above the thin boundary layer is similar to that in the ideal flow.

(Figure 6.1a). In contrast, a real fluid with a nonzero shear viscosity must satisfy a no-slip boundary condition because (4.38) contains second-order spatial derivatives. At sufficiently high Re, there are two primary differences between ideal and real flows over the same object. First, viscous boundary layers containing rotational fluid form on solid surfaces in the real flow, and the thickness of such boundary layers, within which viscous diffusion of vorticity is important, approaches zero as $\mathrm{Re} \to \infty$ (Figure 6.1b). The second difference is the possible formation in the real flow of *separated flow* or *wake* regions that occur when boundary layers leave the surface on which they have developed to create a wider zone of rotational flow (Figure 6.2). Ideal flow theory is not directly applicable to such layers or regions of rotational flow. However, rotational flow regions may be easy to anticipate or identify, and may represent a small fraction of a total flow field so that predictions from ideal flow theory may remain worthwhile even when viscous flow phenomena are present. Further discussion of viscous-flow phenomena is provided in Chapters 8 and 9.

For (4.10) and (6.1) to apply, fluid density ρ must be constant and the flow must be irrotational. If the flow is merely incompressible and contains baroclinic density variations, (4.10) will still be satisfied but (6.1) will not; it will need a body-force term like that in (4.84) and the reference pressure would have to be redefined. If the fluid is a homogeneous compressible gas with sound speed c, the constant density requirement will be satisfied when the Mach number, $M = U/c$ (4.111), of the flow is much less than unity. The irrotationality condition is satisfied when fluid elements enter the flow field of interest without rotation and do not acquire any while they reside in it. Based on Kelvin's circulation theorem (5.11) for constant density flow, this is possible when the body force is conservative and the net viscous force on a fluid element is zero. Thus, a fluid element that is initially irrotational is likely to stay that way unless it enters a boundary layer, wake, or separated flow region where it acquires rotation via viscous diffusion. So, when initially irrotational fluid flows over a solid object, ideal flow theory most readily applies to the *outer* region of the flow away from the object's surface(s) where the flow is irrotational. Viscous flow theory is needed in the *inner* region where viscous diffusion of vorticity is important. Often, at high Re, the outer flow can be approximately predicted by ignoring the existence of viscous boundary layers. With this outer flow prediction, viscous flow equations can be solved for the boundary-layer flow and, under the right conditions, the two solutions can be adjusted until they match in a suitable region of overlap. This approach works well for objects like thin airfoils at low angles of

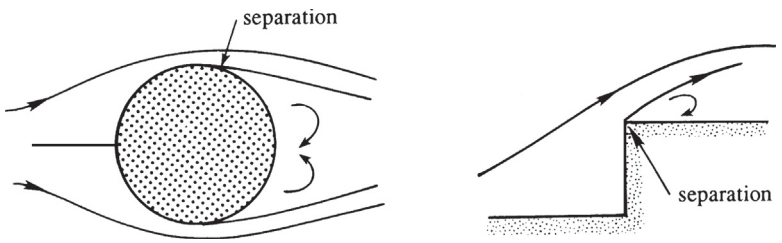

FIGURE 6.2 Schematic drawings of flows with boundary layer separation. (a) Real flow past a cylinder where the boundary layers on the top and bottom of the cylinder leave the surface near its widest point. (b) Real flow past a sharp-cornered obstacle where the boundary layer leaves the surface at the corner. Upstream of the point of separation, ideal flow theory is usually a good approximation of the real flow.

attack when boundary layers remain thin and stay attached all the way to the foil's trailing edge (Figure 6.1b). However, it is not satisfactory when the solid object has such a shape that one or more boundary layers separate from its surface before reaching its downstream edge (Figure 6.2), giving rise to a rotational wake flow or region of separated flow (sometimes called a *bubble*) that is not necessarily thin, no matter how high the Reynolds number. In this case, the limit of a real flow as $\mu \to 0$ does not approach that of an ideal flow ($\mu = 0$). Yet, upstream of boundary layer separation, ideal flow theory may still provide a good approximation of the real flow.

In summary, the theory presented here does not apply to inhomogeneous fluids, high subsonic or supersonic flow speeds, boundary layer flows, wake flows, interior flows, or any flow region where fluid elements rotate. However, the remaining flow possibilities are abundant, and include those that are commercially valuable (flight), naturally important (water waves), or readily encountered in our everyday lives (flow around vehicles; also see Chapters 7 and 14 for further examples).

Steady and unsteady irrotational constant-density flow fields around simple objects and through simple geometries in two and three dimensions are the subjects of this chapter. All the coordinate systems presented in Figure 3.3 are utilized herein.

6.2. TWO-DIMENSIONAL STREAM FUNCTION AND VELOCITY POTENTIAL

The two-dimensional incompressible continuity equation,

$$\partial u/\partial x + \partial v/\partial y = 0, \tag{6.2}$$

is identically satisfied when u,v-velocity components are determined from a single scalar function ψ:

$$u \equiv \partial\psi/\partial y, \text{ and } v \equiv -\partial\psi/\partial x. \tag{6.3}$$

The function $\psi(x,y)$ is the stream function in two dimensions. Along a curve of $\psi = \text{constant}$, $d\psi = 0$, and this implies

$$0 = d\psi = \frac{\partial\psi}{\partial x}dx + \frac{\partial\psi}{\partial y}dy = -v dx + u dy, \text{ or } \left(\frac{dy}{dx}\right)_{\psi=const} = \frac{v}{u},$$

which is the definition of a streamline in two dimensions. The vorticity ω_z in a flow described by ψ is:

$$\frac{\partial v}{\partial x} - \frac{\partial u}{\partial y} = \omega_z = \frac{\partial}{\partial x}\left(-\frac{\partial\psi}{\partial x}\right) - \frac{\partial}{\partial y}\left(\frac{\partial\psi}{\partial y}\right) = -\nabla^2\psi. \tag{6.4}$$

In constant-density irrotational flow, ω_z will be zero everywhere except at the locations of irrotational vortices. Thus, we are interested in solutions of

$$\nabla^2\psi = 0, \text{ and } \nabla^2\psi = -\Gamma\delta(x - x')\delta(y - y'), \tag{6.5, 6.6}$$

where δ is the Dirac delta-function (see Appendix B.4), and $\mathbf{x}' = (x', y')$ is the location of an ideal irrotational vortex of strength Γ.

In an unbounded domain, the most elementary nontrivial solutions of (6.5) and (6.6) are

$$\psi = -Vx + Uy, \text{ and } \psi = -\frac{\Gamma}{2\pi}\ln\sqrt{(x-x')^2+(y-y')^2}, \tag{6.7, 6.8}$$

respectively. These correspond to uniform fluid velocity with horizontal component U and vertical component V, and to the flow induced by an irrotational vortex located at $\mathbf{x}'$ (see Exercise 6.1).

These two-dimensional stream function results have been obtained by considering incompressibility first, and irrotationality second. An equivalent formulation of two-dimensional ideal flow that leads to a different scalar function is possible when incompressibility and irrotationality are considered in the other order. The condition of irrotationality in two dimensions is

$$\partial v/\partial x - \partial u/\partial y = 0, \tag{6.9}$$

and it is identically satisfied when u,v-velocity components are determined from a single scalar function ϕ:

$$u \equiv \partial\phi/\partial x, \text{ and } v \equiv \partial\phi/\partial y. \tag{6.10}$$

The function $\phi(x,y)$ is known as the *velocity potential* in two dimensions because (6.10) implies $\nabla\phi = \mathbf{u}$. In fact, a velocity potential must exist in all irrotational flows, so such flows are frequently called *potential flows*. Curves of $\phi =$ constant are defined by

$$0 = d\phi = \frac{\partial\phi}{\partial x}dx + \frac{\partial\phi}{\partial y}dy = udx + vdy \text{ or } \left(\frac{dy}{dx}\right)_{\phi=const} = -\frac{u}{v},$$

and are perpendicular to streamlines. When using $\phi(x,y)$, the condition for incompressibility becomes:

$$\frac{\partial u}{\partial x} + \frac{\partial v}{\partial y} = \frac{\partial}{\partial x}\left(\frac{\partial\phi}{\partial x}\right) + \frac{\partial}{\partial y}\left(\frac{\partial}{\partial y}\right)\phi = \nabla^2\phi = q(x,y), \tag{6.11}$$

where $q(x,y)$ is the spatial distribution of the source strength in the flow field. Of course, in real incompressible flows, $q(x,y) = 0$; however, ideal point sources and sinks of fluid are useful idealizations that allow the flow around objects of various shapes to be determined. These point sources and sinks are the ϕ-field equivalents of positive- and negative-circulation ideal vortices in flow fields described by ψ. Thus, we are interested in solutions of

$$\nabla^2\phi = 0, \text{ and } \nabla^2\phi = m\delta(x-x')\delta(y-y'), \tag{6.12, 6.13}$$

where m is a constant that sets the strength of the singularity at $\mathbf{x}'$.

In an unbounded domain, the most elementary solutions of (6.12) and (6.13) are

$$\phi = Ux + Vy, \text{ and } \phi = \frac{m}{2\pi}\ln\sqrt{(x-x')^2+(y-y')^2}, \tag{6.14, 6.15}$$

respectively. These correspond to uniform fluid velocity with horizontal component U and vertical component V, and to the flow induced by an ideal point source of strength m located at $\mathbf{x}'$ (see Exercise 6.3). Here, m is the source's volume flow rate per unit depth perpendicular to the plane of the flow.

Either ψ or ϕ can provide a complete description of a two-dimensional ideal flow, and they can be combined to form a complex potential that follows the theory of *harmonic* functions (see Section 6.4). In addition, ψ is readily extended to rotational flows while ϕ is readily extended to unsteady and three-dimensional flows.

Boundary conditions must be considered to extend the elementary ideal flow solutions (6.7), (6.8), (6.14), and (6.15) to more interesting geometries. The boundary conditions normally encountered in irrotational flows are as follows.

(1) *No flow through a solid surface*. The component of fluid velocity normal to a solid surface must equal the velocity of the boundary normal to itself. This can be stated as $\mathbf{n}\cdot\mathbf{U_s} = (\mathbf{n}\cdot\mathbf{u})_{on\ the\ surface}$, where $\mathbf{n}$ is the surface's normal and $\mathbf{U}_s$ is the velocity of the surface at the point of interest. For a stationary body, this condition reduces to $(\mathbf{n}\cdot\mathbf{u})_{on\ the\ surface} = 0$, which implies:

$$\partial\phi/\partial n = 0 \text{ or } \partial\psi/\partial s = 0 \text{ on the surface}, \tag{6.16}$$

where s is the arc-length along the surface, and n is the surface-normal coordinate. However, $\partial\psi/\partial s$ is also zero along a streamline. Thus, a stationary solid boundary in an ideal flow must also be a streamline. Therefore, if any ideal-flow streamline is replaced by a stationary solid boundary having the same shape, then the remainder of the flow is not changed.

(2) *Recovery of conditions at infinity*. For the typical case of a body immersed in a uniform fluid flowing in the x direction with speed U, the condition far from the body is

$$\partial\phi/\partial x = U, \text{ or } \partial\psi/\partial y = U. \tag{6.17}$$

When $U = 0$, the fluid far from the body is said to be quiescent.

Solving the Laplace equation, (6.5) or (6.12), with complicated-geometry boundary conditions like (6.16) and (6.17) requires numerical techniques. Historically, irrotational flow theory was developed by finding functions that satisfy the Laplace equation and then determining the boundary conditions met by those functions. Since the Laplace equation is linear, any superposition of known solutions provides another solution, but the superposition of two or more solutions may satisfy different boundary conditions than any of the constituents of the superposition. Thus, through collection and combination, a rich variety of interesting ideal-flow solutions has emerged. This solution-construction approach to ideal flow theory is adopted in this chapter, except in Sections 6.7 and 6.8 where numerical methods for solving (6.5) or (6.12) subject to (6.16) or (6.17) are presented.

After a solution of the Laplace equation has been obtained, the velocity components are determined by taking derivatives of ϕ or ψ. Then, the conservation of momentum equation (6.1) is satisfied for steady flow by determining pressure from the Bernoulli equation:

$$p + \frac{1}{2}\rho|\mathbf{u}|^2 = p + \frac{1}{2}\rho\left(u^2 + v^2\right) = p + \frac{1}{2}\rho|\nabla\phi|^2 = p + \frac{1}{2}\rho|\nabla\psi|^2 = const. \tag{6.18}$$

For unsteady flow, the term $\rho(\partial\phi/\partial t)$ must be added (see Exercise 6.4). With this procedure, solutions of (4.10) and (6.1) for $\mathbf{u}$ and p are obtained for ideal flows in a simple manner even though (6.1) is nonlinear.

For quick reference, the important equations in planar polar coordinates are:

$$\frac{1}{r}\frac{\partial}{\partial r}(ru_r)+\frac{1}{r}\frac{\partial u_\theta}{\partial \theta}=0 \qquad \text{(continuity)}, \tag{6.19}$$

$$\frac{1}{r}\frac{\partial}{\partial r}(ru_\theta)-\frac{1}{r}\frac{\partial u_r}{\partial \theta}=0 \quad \text{(irrotationality)}, \tag{6.20}$$

$$u_r=\frac{\partial \phi}{\partial r}=\frac{1}{r}\frac{\partial \psi}{\partial \theta}, \tag{6.21}$$

$$u_\theta=\frac{1}{r}\frac{\partial \phi}{\partial \theta}=-\frac{\partial \psi}{\partial r}, \tag{6.22}$$

$$\nabla^2\psi=\frac{1}{r}\frac{\partial}{\partial r}\left(r\frac{\partial \psi}{\partial r}\right)+\frac{1}{r^2}\frac{\partial^2\psi}{\partial \theta^2}=0, \text{ and } \nabla^2\phi=\frac{1}{r}\frac{\partial}{\partial r}\left(r\frac{\partial \phi}{\partial r}\right)+\frac{1}{r^2}\frac{\partial^2\phi}{\partial \theta^2}=0. \tag{6.23a, 6.23b}$$

6.3. CONSTRUCTION OF ELEMENTARY FLOWS IN TWO DIMENSIONS

In this section, elementary solutions of the Laplace equation are developed and then superimposed to produce a variety of geometrically simple ideal flows in two dimensions.

First consider polynomial solutions of the Laplace equation in Cartesian coordinates. A zero-order polynomial, ψ or $\phi=$ constant, is not interesting since with either field function the result is $\mathbf{u}=0$. First-order polynomial solutions are given by (6.7) and (6.14), and these solutions represent spatially uniform velocity fields, $\mathbf{u}=(U,V)$. Quadratic functions in x and y are the next possibilities, and there are two of these:

$$\psi=2Axy \text{ or } \phi=2Axy, \text{ and } \psi=A\left(x^2-y^2\right) \text{ or } \phi=A\left(x^2-y^2\right), \tag{6.24–6.27}$$

where A is a constant. (The reason for the two in (6.24) and (6.25) will be clear in the next section.) Here we will only construct the flow fields for $2Axy$. Production of flow-field results for ψ and $\phi=A(x^2-y^2)$ is left as an exercise.

Examine $\psi=2Axy$ first, and by direct differentiation find $u=2Ax$, and $v=-2Ay$. Thus, for $A>0$, the flow is toward the origin along the y-axis, away from it along the x-axis, and the streamlines are hyperbolae given by $xy=\psi/2A$ (Figure 6.3). Considering the first quadrant only, this is flow in a 90° corner. Now consider $\phi=2Axy$, and by direct differentiation find $u=2Ay$, and $v=2Ax$. The equipotential lines are hyperbolae given by $xy=\phi/2A$. The flow is away from the origin along the line $y=x$ and toward it along the line $y=-x$. Thus, $\phi=2Axy$ produces a flow that is equivalent to that of $\psi=2Axy$ after a 45° rotation. Interestingly, higher-order polynomial solutions lead to flows in smaller-angle corners, while fractional powers lead to flows in larger-angle corners (see Section 6.4 and Exercises 6.6 and 6.7).

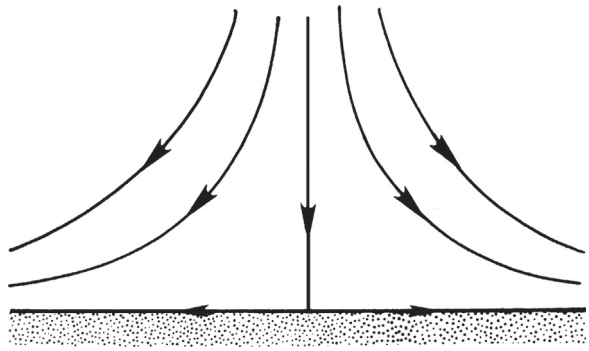

FIGURE 6.3 Stagnation point flow represented by $\psi = 2Axy$. Here the flow impinges on the flat surface from above. The stagnation point is located where the single vertical streamline touches the horizontal surface.

The next set of solutions to consider are (6.8) and (6.15) with $x' = y' = 0$. In this case, curves of $\psi = -(\Gamma/2\pi)\ln\sqrt{x^2+y^2} = const.$ are circles centered on the origin of coordinates (Figure 6.4), and direct differentiation of (6.8) produces:

$$u = \frac{\partial}{\partial y}\left(-\frac{\Gamma}{2\pi}\ln\sqrt{x^2+y^2}\right) = -\frac{\Gamma}{2\pi}\frac{y}{x^2+y^2} = -\frac{\Gamma}{2\pi r}\sin\theta\,, \text{ and}$$

$$v = -\frac{\partial}{\partial x}\left(-\frac{\Gamma}{2\pi}\ln\sqrt{x^2+y^2}\right) = +\frac{\Gamma}{2\pi}\frac{x}{x^2+y^2} = \frac{\Gamma}{2\pi r}\cos\theta,$$

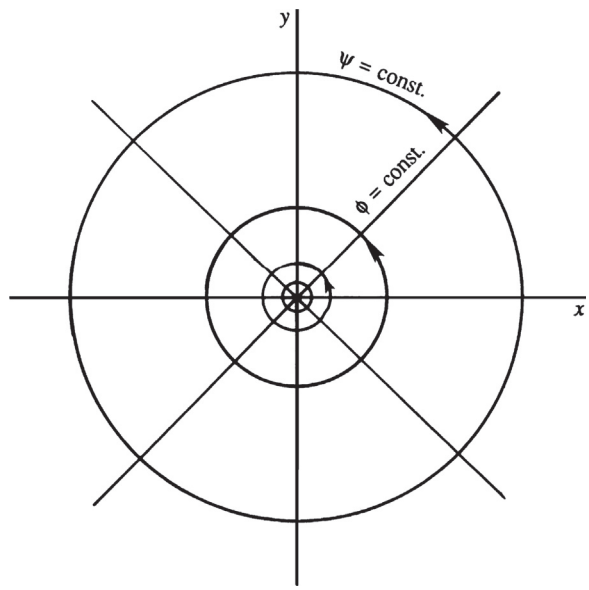

FIGURE 6.4 The flow field of an ideal vortex located at the origin of coordinates. The streamlines are circles and the potential lines are radials. Here, the vortex line is perpendicular to the x-y plane.

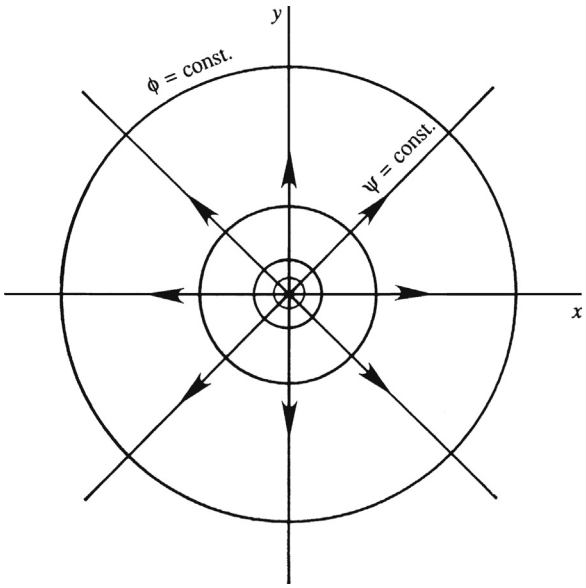

FIGURE 6.5 The flow field of an ideal source located at the origin of coordinates in two dimensions. The streamlines are radials and the potential lines are circles.

where r and θ are defined in Figure 3.3a. These results may be rewritten using the outcome of Example 2.1 as $u_r = 0$ and $u_\theta = \Gamma/2\pi r$, which is the flow field of the ideal irrotational vortex (5.2). Similarly, curves of $\phi = (m/2\pi)\ln\sqrt{x^2+y^2} = const.$ are circles centered on the origin of coordinates (Figure 6.5), and direct differentiation of (6.8) produces:

$$u = \frac{\partial}{\partial x}\left(\frac{m}{2\pi}\ln\sqrt{x^2+y^2}\right) = \frac{m}{2\pi}\frac{x}{x^2+y^2} = \frac{m}{2\pi r}\cos\theta, \text{ and}$$

$$v = \frac{\partial}{\partial y}\left(\frac{m}{2\pi}\ln\sqrt{x^2+y^2}\right) = \frac{m}{2\pi}\frac{y}{x^2+y^2} = \frac{m}{2\pi r}\sin\theta.$$

These results may be rewritten as $u_r = m/2\pi r$ and $u_\theta = 0$, which is purely radial flow away from the origin (Figure 6.5). Here, $\nabla\cdot\mathbf{u}$ is zero everywhere except at the origin. Thus, this potential represents flow from an ideal incompressible point source for $m > 0$, or sink for $m < 0$, that is located at $r = 0$ in two dimensions.

A source of strength $+m$ at $(-\varepsilon, 0)$ and sink of strength $-m$ at $(+\varepsilon, 0)$, can be considered together

$$\phi = \frac{m}{2\pi}\ln\sqrt{(x+\varepsilon)^2+y^2} - \frac{m}{2\pi}\ln\sqrt{(x-\varepsilon)^2+y^2}$$

to obtain the potential for a *doublet* in the limit that $\varepsilon \to 0$ and $m \to \infty$, so that the dipole strength vector

$$\mathbf{d} = \sum_{sources} \mathbf{x}_i m_i = -\varepsilon\mathbf{e}_x m + \varepsilon\mathbf{e}_x(-m) = -2m\varepsilon\mathbf{e}_x \tag{6.28}$$

remains constant. Here, the dipole strength points from the sink toward the source. As $\varepsilon \to 0$, the logarithm of the square roots can be simplified:

$$\ln\sqrt{(x \pm \varepsilon)^2 + y^2} = \ln r + \ln\sqrt{1 \pm 2\varepsilon x/r^2 + \varepsilon^2/r^2} = \ln r + \ln(1 \pm \varepsilon x/r^2 + \ldots) \cong \ln(r) \pm \varepsilon x/r^2,$$

where $r^2 = x^2 + y^2$, so

$$\lim_{\varepsilon \to 0} \lim_{m \to \infty} \phi \cong \frac{m}{2\pi}\left(\ln r + \frac{\varepsilon x}{r^2} + \ldots - \ln r + \frac{\varepsilon x}{r^2} + \ldots\right) = \frac{m\varepsilon}{\pi}\frac{x}{r^2} = -\frac{\mathbf{d}\cdot\mathbf{x}}{2\pi r^2} = \frac{|\mathbf{d}|}{2\pi}\frac{\cos\theta}{r}. \tag{6.29}$$

The doublet flow field is illustrated in Figure 6.6. The stream function for the doublet can be derived from (6.29) (Exercise 6.9).

The flows described by (6.7), (6.14), and (6.24) through (6.27) are solutions of the Laplace equation. The flows described by (6.8), (6.15), and (6.29) are singular at the origin and satisfy the Laplace equation for $r > 0$. Perhaps the most common and useful superposition of these solutions involves the combining of a uniform stream parallel to the x-axis, $\psi = Uy$ or $\phi = Ux$,

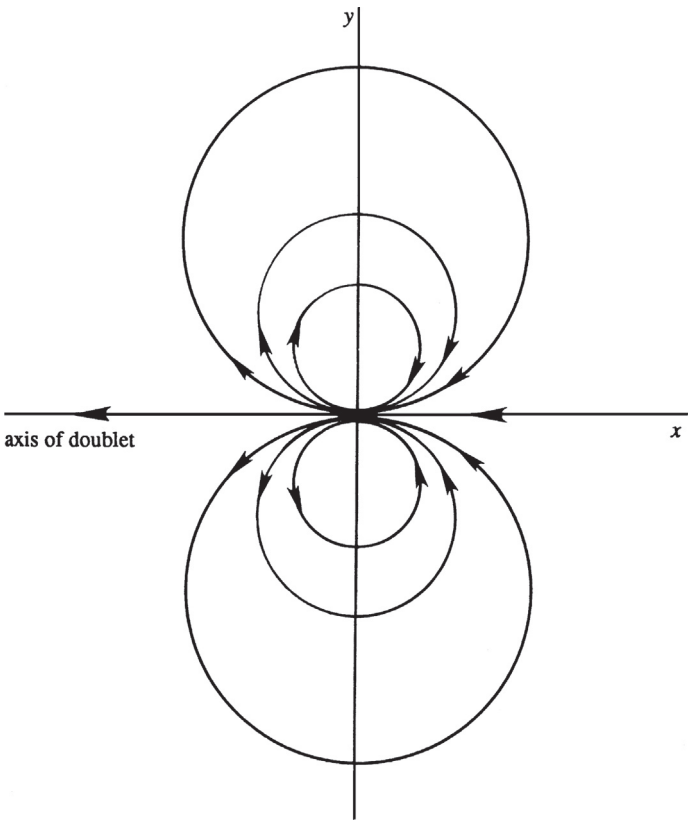

FIGURE 6.6 The flow field of an ideal doublet that points along the negative x-axis. The net source strength is zero so all streamlines begin and end at the origin. In this flow, the streamlines are circles tangent to the x-axis at the origin.

and one or more of the singular solutions. The simplest example is the combination of a source and a uniform stream, which can be written in Cartesian and polar coordinates as:

$$\phi = Ux + \frac{m}{2\pi}\ln\sqrt{x^2+y^2} = Ur\cos\theta + \frac{m}{2\pi}\ln r, \text{ or} \tag{6.30}$$

$$\psi = Uy + \frac{m}{2\pi}\tan^{-1}\left(\frac{y}{x}\right) = Ur\sin\theta + \frac{m}{2\pi}\theta. \tag{6.31}$$

Here the velocity field is:

$$u = U + \frac{m}{2\pi}\frac{x}{x^2+y^2} \quad \text{and} \quad v = \frac{m}{2\pi}\frac{y}{x^2+y^2},$$

and streamlines are shown in Figure 6.7. The stagnation point is located at $x = -a = -m/2\pi U$, and $y = 0$, and the value of the stream function on the stagnation streamline is $\psi = m/2$.

The streamlines that emerge vertically from the stagnation point (the darker curves in Figure 6.7) form a semi-infinite body with a smooth nose, generally called a *half-body*. These stagnation streamlines divide the field into regions external and internal to the half-body. The internal flow consists entirely of fluid emanating from the source, and the external region contains fluid from upstream of the source. The half-body resembles several practical shapes, such as the leading edge of an airfoil or the front part of a bridge pier; the upper half of the flow resembles the flow over a cliff or a side contraction in a wide channel. The half-width of the body, h, can be found from (6.31) with $\psi = m/2$:

$$h = m(\pi - \theta)/2\pi U.$$

Far downstream ($\theta \to 0$), the half-width tends to $h_{max} = m/2U$ (Figure 6.7).

The pressure distribution on the half-body can be found from Bernoulli's equation, (6.18) with $const. = p_\infty + \rho U^2/2$, and is commonly reported as a dimensionless excess pressure via the *pressure coefficient* C_p or Euler number (4.106):

$$C_p = \frac{p - p_\infty}{\frac{1}{2}\rho U^2} = 1 - \frac{|\mathbf{u}|^2}{U^2}. \tag{6.32}$$

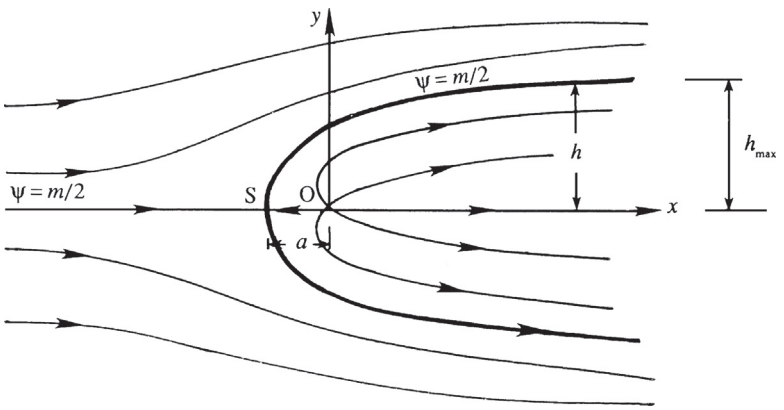

FIGURE 6.7 Ideal flow past a two-dimensional half-body formed from a horizontal free stream and a point source at the origin. The boundary streamline, shown as a darker curve, is given by $\psi = m/2$.

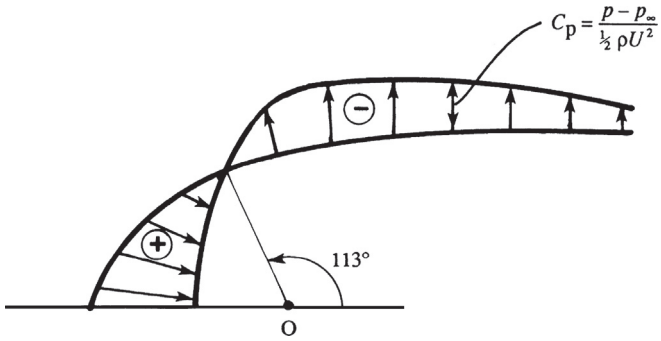

FIGURE 6.8 Pressure distribution in ideal flow over the half-body shown in Figure 6.7. Pressure excess near the nose is indicated by the circled "+" and pressure deficit elsewhere is indicated by the circled "−".

A plot of C_p on the surface of the half-body is given in Figure 6.8, which shows that there is pressure excess near the nose of the body and a pressure deficit beyond it. It is easy to show by integrating p over the surface that the net pressure force is zero (Exercise 6.13).

As a second example of flow construction via superposition, consider a horizontal free stream U and a doublet with strength $\mathbf{d} = -2\pi U a^2 \mathbf{e}_x$:

$$\phi = Ux + \frac{Ua^2 x}{x^2 + y^2} = U\left(r + \frac{a^2}{r}\right)\cos\theta, \text{ or } \psi = Uy - \frac{Ua^2 y}{x^2 + y^2} = U\left(r - \frac{a^2}{r}\right)\sin\theta. \tag{6.33}$$

Here, $\psi = 0$ at $r = a$ for all values of θ, showing that the streamline $\psi = 0$ represents a circular cylinder of radius a. The streamline pattern is shown in Figure 6.9 (and Figure 3.2a). In this flow, the net source strength is zero, so the cylindrical body is closed and does not extend downstream. The velocity field is:

$$u_r = U\left(1 - \frac{a^2}{r^2}\right)\cos\theta, \text{ and } u_\theta = -U\left(1 + \frac{a^2}{r^2}\right)\sin\theta. \tag{6.34}$$

The velocity components on the surface of the cylinder are $u_r = 0$ and $u_\theta = -2U\sin\theta$, so the cylinder-surface pressure coefficient is:

$$C_p(r = a, \theta) = 1 - 4\sin^2\theta, \tag{6.35}$$

and this is shown by the continuous line in Figure 6.10. There are stagnation points on the cylinder's surface at r-θ coordinates, $(a, 0)$ and (a, π). The cylinder-surface pressure minima occur at r-θ coordinates $(a, \pm\pi/2)$ where the surface flow speed is maximum. The symmetry of the pressure distribution implies that there is no net pressure force on the cylinder. In fact, a general result of two-dimensional ideal flow theory is that a steadily moving body experiences no drag. This result is at variance with observations and is sometimes known as *d'Alembert's paradox*. The existence of real-flow tangential stress on a solid surface, commonly known as *skin friction*, is not the only reason for the discrepancy. For blunt bodies such as a cylinder, most of the drag comes from flow separation and the formation of a wake, which is likely to be unsteady or even turbulent. When a wake is present, the flow loses fore-aft

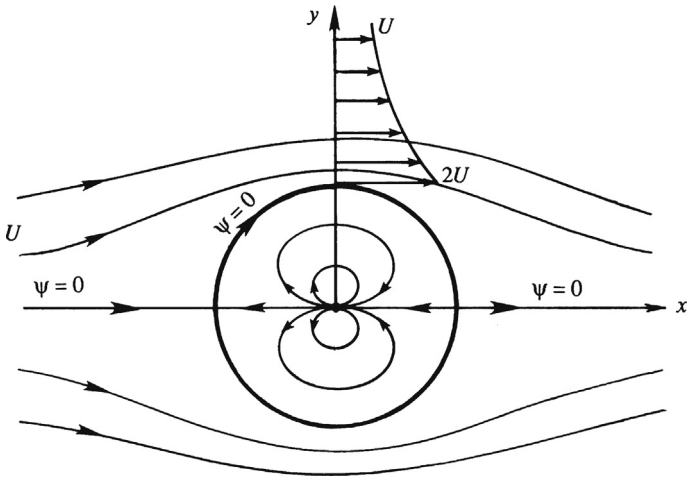

FIGURE 6.9 Idea flow past a circular cylinder without circulation. This flow field is formed by combining a horizontal uniform stream flowing in the $+x$ direction with a doublet pointing in the $-x$ direction. The streamline that passes through the two stagnation points and forms the body surface is given by $\psi = 0$.

symmetry, and the surface pressure on the downstream side of the object is smaller than that predicted by ideal flow theory (Figure 6.10), resulting in pressure drag. These facts will be discussed further in Chapter 9.

As discussed in Section 3.3, the flow due to a cylinder moving steadily through a fluid appears unsteady to an observer at rest with respect to the fluid at infinity. This flow is shown in Figure 3.3b and can be obtained by superposing a uniform stream in the negative x direction with the flow shown in Figure 6.9. The resulting instantaneous streamline pattern is simply that of a doublet, as is clear from the decomposition shown in Figure 6.11.

FIGURE 6.10 Comparison of irrotational and observed pressure distributions over a circular cylinder. Here 0° is the most upstream point of the cylinder and 180° is the most downstream point. The observed distribution changes with the Reynolds number; a typical behavior at high Re is indicated by the dashed line.

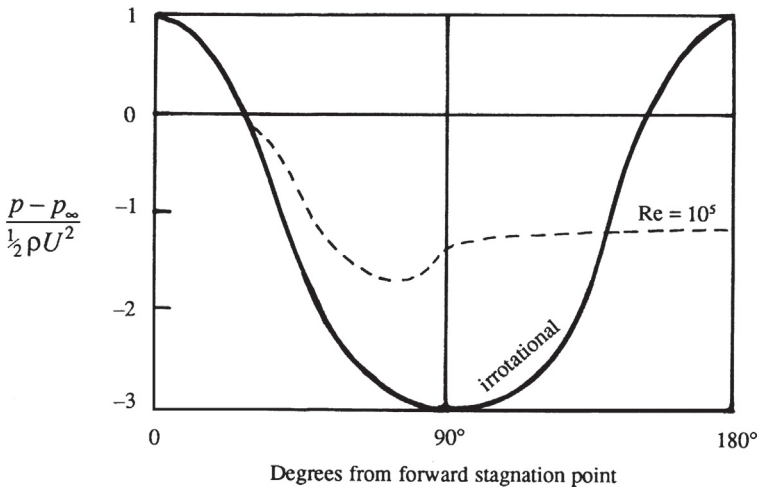

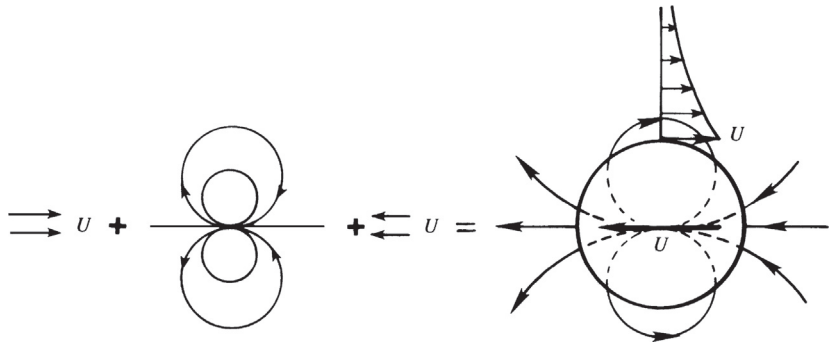

FIGURE 6.11 Decomposition of the irrotational flow pattern due to a moving cylinder. Here a horizontal free stream of $+U$ and doublet form a cylinder. When a uniform stream of $-U$ is added, the flow field of a moving cylinder is obtained.

Although there is no net drag force on a circular cylinder in steady irrotational flow, there may be a lateral or lift force perpendicular to the free stream when circulation is added. Consider the flow field (6.33) with the addition of a point vortex of circulation $-\Gamma$[1] at the origin that induces a *clockwise* velocity:

$$\psi = U\left(r - \frac{a^2}{r}\right)\sin\theta + \frac{\Gamma}{2\pi}\ln\left(\frac{r}{a}\right). \tag{6.36}$$

Here, a has been added to the logarithm's argument to make it dimensionless.

Figure 6.12 shows the resulting streamline pattern for various values of Γ. The close streamline spacing and higher velocity on top of the cylinder is due to the addition of velocities from the clockwise vortex and the uniform stream. In contrast, the smaller velocities at the bottom of the cylinder are a result of the vortex field counteracting the uniform stream. Bernoulli's equation consequently implies a higher pressure below the cylinder than above it, and this pressure difference leads to an upward lift force on the cylinder.

The tangential velocity component at any point in the flow is

$$u_\theta = -\frac{\partial\psi}{\partial r} = -U\left(1 + \frac{a^2}{r^2}\right)\sin\theta - \frac{\Gamma}{2\pi r}.$$

At the surface of the cylinder, the fluid velocity is entirely tangential and is given by

$$u_\theta(r = a, \theta) = -2U\sin\theta - \Gamma/2\pi a, \tag{6.37}$$

which vanishes if

$$\sin\theta = -\Gamma/4\pi aU. \tag{6.38}$$

For $\Gamma < 4\pi aU$, two values of θ satisfy (6.38), implying that there are two stagnation points on the cylinder's surface. The stagnation points progressively move down as Γ increases (Figure 6.12) and coalesce when $\Gamma = 4\pi aU$. For $\Gamma > 4\pi aU$, the stagnation point moves out

[1]This minus sign is necessary to achieve the usual fluid dynamic result given by (6.40).

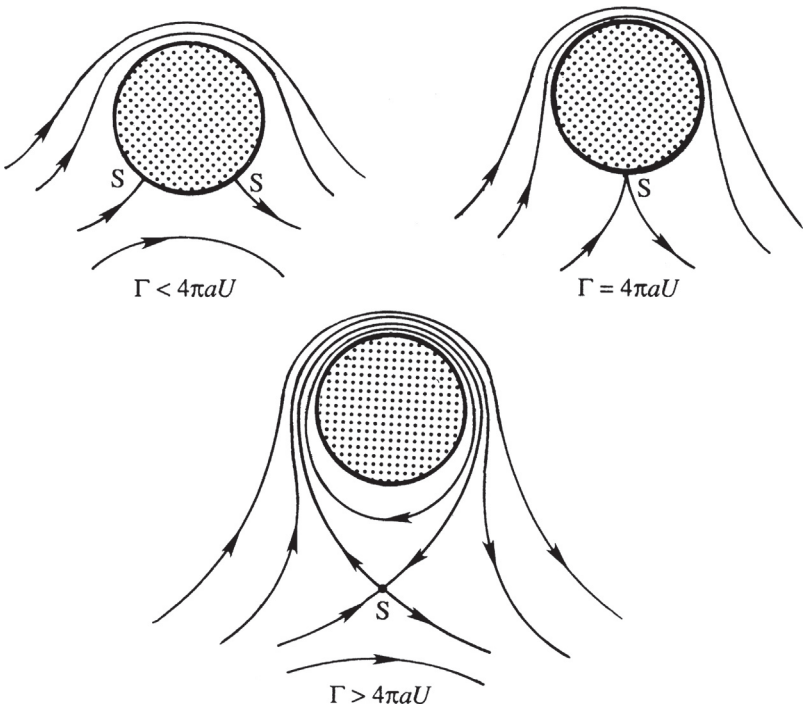

FIGURE 6.12 Irrotational flow past a circular cylinder for different circulation values. Here S represents the stagnation point(s) in the flow. (a) At low values of the circulation, there are two stagnation points on the surface of the cylinder. (b) When the circulation is equal to $4\pi aU$, there is one stagnation point on the surface of the cylinder. (c) When the circulation is even greater, there is one stagnation point below the cylinder.

into the flow along the negative y-axis. The radial distance of the stagnation point in this case is found from

$$u_\theta(r, \theta = -\pi/2) = U\left(1 + \frac{a^2}{r^2}\right) - \frac{\Gamma}{2\pi r} = 0, \text{ or } r = \frac{1}{4\pi U}\left[\Gamma \pm \sqrt{\Gamma^2 - (4\pi aU)^2}\right],$$

one root of which has $r > a$; the other root corresponds to a stagnation point inside the cylinder.

The cylinder surface pressure is found from (6.18) with $const. = p_\infty + \rho U^2/2$, and (6.37) to be

$$p(r = a, \theta) = p_\infty + \frac{1}{2}\rho\left[U^2 - \left(-2U\sin\theta - \frac{\Gamma}{2\pi a}\right)^2\right]. \tag{6.39}$$

The upstream-downstream symmetry of the flow implies that the pressure force on the cylinder has no stream-wise component. The lateral pressure force (per unit length perpendicular to the flow plane) is

$$L = -\int_0^{2\pi} p(r = a, \theta)\mathbf{n}dl \cdot \mathbf{e}_y = -\int_0^{2\pi} p(r = a, \theta)\sin\theta a d\theta,$$

where $\mathbf{n} = \mathbf{e}_r$ is the outward normal from the cylinder, and $dl = ad\theta$ is a surface element of the cylinder's cross section; L is known as the *lift* force in aerodynamics (Figure 6.13). Evaluating the integral using (6.39) produces:

$$L = \rho U \Gamma. \tag{6.40}$$

It is shown in Section 6.5 that (6.40) holds for irrotational flow around *any* two-dimensional object; it is not just for circular cylinders. The result that L is proportional to Γ is of fundamental importance in aerodynamics. Equation (6.40) was proved independently by the German mathematician Wilhelm Kutta and the Russian aerodynamist Nikolai Zhukhovsky just after 1900; it is called the *Kutta-Zhukhovsky lift theorem*. (Older Western texts transliterated Zhukhovsky's name as Joukowsky.) The interesting question of how certain two-dimensional shapes, such as an airfoil, develop circulation when placed in a moving fluid is discussed in Chapter 14. It is shown there that fluid viscosity is responsible for the development of circulation. The magnitude of circulation, however, is independent of viscosity but does depend on the flow speed U, and the shape and orientation of the object.

For a circular cylinder, the only way to develop circulation is by rotating it. Although viscous effects are important in this case, the observed flow pattern for *large* values of cylinder rotation displays a striking similarity to the ideal flow pattern for $\Gamma > 4\pi aU$; see Figure 3.25 in the book by Prandtl (1952). For lower rates of cylinder rotation, the retarded flow in the boundary layer is not able to overcome the adverse pressure gradient behind the cylinder, leading to separation; the real flow is therefore rather unlike the irrotational pattern. However, even in the presence of separation, observed flow speeds are higher on the upper surface of the cylinder, implying a lift force.

A second reason for the presence of lift on a rotating cylinder is the flow asymmetry generated by a delay of boundary layer separation on the upper surface of the cylinder. The contribution of this mechanism is small for two-dimensional objects such as the circular cylinder,

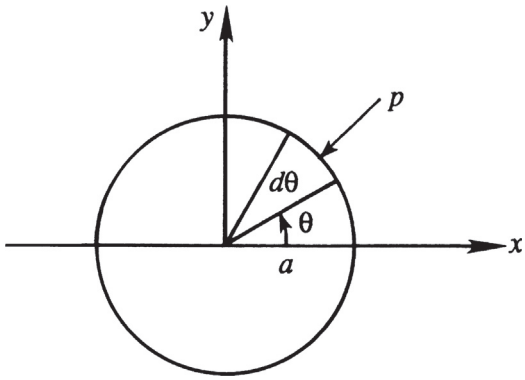

FIGURE 6.13 Calculation of pressure force on a circular cylinder. Surface pressure forces on top of the cylinder, where **n** has a positive vertical component, push the cylinder down. Thus the surface integral for the lift force applied by the fluid to the cylinder contains a minus sign.

but it is the only mechanism for side forces experienced by spinning three-dimensional objects like sports balls. The interesting question of why spinning balls follow curved paths is discussed in Section 9.9. The lateral force experienced by rotating bodies is called the *Magnus effect*.

Two-dimensional ideal flow solutions are commonly not unique and the topology of the flow domain determines uniqueness. Simply stated, a two-dimensional ideal flow solution is unique when any closed contour lying entirely within the fluid can be reduced to a point by continuous deformation without ever cutting through a flow-field boundary. Such fluid domains are *singly connected*. Thus, fluid domains, like those shown in Figures 6.9 and 6.12, that entirely encircle an object may not provide unique ideal flow solutions based on boundary conditions alone. In particular, consider the ideal flow (6.36) depicted in Figure 6.12 for various values of Γ. All satisfy the *same* boundary condition on the solid surface ($u_r = 0$) and at infinity ($\mathbf{u} = U\mathbf{e}_x$). The ambiguity occurs in these domains because there exist closed contours lying entirely within the fluid that cannot be reduced to a point, and on these contours a nonzero circulation can be computed. Fortunately, this ambiguity may often be resolved by considering real-flow effects. For example, the circulation strength that should be assigned to a streamlined object in two-dimensional ideal flow can be determined by applying the viscous flow–based *Kutta* condition at the object's trailing edge. This point is further explained in Chapter 14.

Another important consequence of the superposition principle for ideal flow is that it allows boundaries to be built into ideal flows through the method of images. For example, if the flow of interest in an unbounded domain is the solution of $\nabla^2\psi_1 = -\omega_1(x,y)$, then $\nabla^2\psi_2 = -\omega_1(x,y) + \omega_1(x,-y)$ will determine the solution for the same vorticity distribution with a solid wall along the x-axis. Here, $\psi_2 = \psi_1(x,y) - \psi_1(x,-y)$, so that the *zero* streamline, $\psi_2 = 0$, occurs on $y = 0$ (Figure 6.14). Similarly, if the flow of interest in an unbounded domain is the solution of $\nabla^2\phi_1 = q_1(x,y)$, then $\nabla^2\phi_2 = q_1(x,y) + q_1(x,-y)$ will determine the solution for the same source distribution with a solid wall along the x-axis. Here, $\phi_2 = \phi_1(x,y) + \phi_1(x,-y)$ so that $v = \partial\phi_2/\partial y = 0$ on $y = 0$ (Figure 6.15).

As an example of the method of images, consider the flow induced by an ideal source of strength m a distance a from a straight vertical wall (Figure 6.16). Here an image source of the same strength and sign is needed a distance a on the other side of the wall. The stream function and potential for this flow are:

$$\psi = \frac{m}{2\pi}\left[\tan^{-1}\left(\frac{y}{x+a}\right) + \tan^{-1}\left(\frac{y}{x-a}\right)\right] \text{ and } \phi = \frac{m}{2\pi}\left[\ln\sqrt{(x+a)^2+y^2} + \ln\sqrt{(x-a)^2+y^2}\right], \tag{6.41}$$

FIGURE 6.14 Illustration of the method of images for the flow near a horizontal wall generated by a vorticity distribution. An image distribution of equal strength and opposite sign mimics the effect of the solid wall.

FIGURE 6.15 Illustration of the method of images for the flow near a horizontal wall generated by a source distribution. An image distribution of equal strength mimics the effect of the solid wall.

respectfully. After some rearranging and use of the two-angle formula for the tangent function, the equation for the streamlines may be found:

$$x^2 - y^2 - 2xy \cot(2\pi\psi/m) = a^2.$$

The x and y axes form part of the streamline pattern, with the origin as a stagnation point. This flow represents three interesting situations: flow from two equal sources (all of Figure 6.16), flow from a source near a flat vertical wall (right half of Figure 6.16), and flow through a narrow slit at $x = a$ into a right-angled corner (first quadrant of Figure 6.16).

The method of images can commonly be extended to circular boundaries by allowing more than one image vortex or source (Exercises 5.14, 6.26), and to unsteady flows as long as the image distributions of vorticity or source strength move appropriately. Unsteady two-dimensional ideal flow merely involves the inclusion of time as an independent variable in ψ or ϕ, and the addition of $\rho(\partial\phi/\partial t)$ in the Bernoulli equation (see Exercise 6.4). The following example, which validates the free-vortex results stated in Chapter 5.7, illustrates these changes.

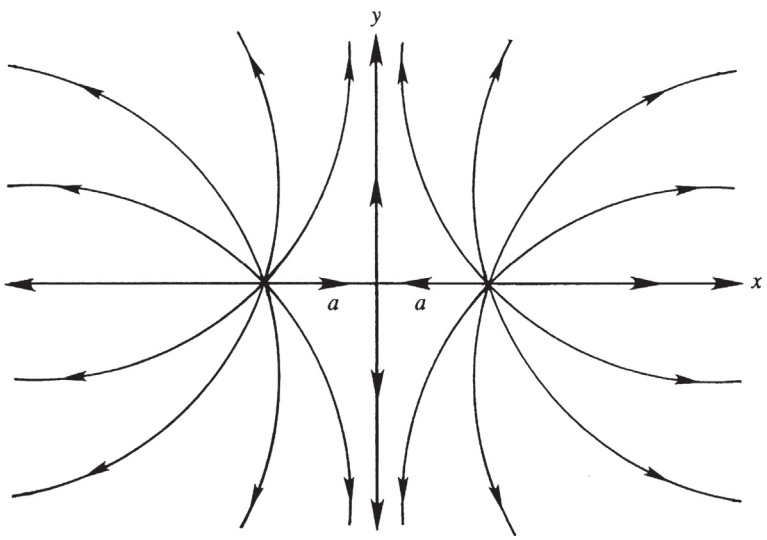

FIGURE 6.16 Ideal flow from two equal sources placed at $x = \pm a$. The origin is a stagnation point. The vertical axis is a streamline and may be replaced by a solid surface. This flow field further illustrates the method of images.

EXAMPLE 6.1

At $t = 0$, an ideal free vortex with strength $-\Gamma$ is located at point A near a flat solid vertical wall as shown in Figure 5.14. If the x,y-coordinates of A are (h,0) and the fluid far from the vortex is quiescent at pressure p_∞, determine the trajectory $\boldsymbol{\xi}(t) = (\xi_x, \xi_y)$ of the vortex, and the pressure at the origin of coordinates as a function of time.

Solution

From the method of images, the stream function for this flow field will be:

$$\psi(x,y,t) = \frac{\Gamma}{2\pi}\left[-\ln\sqrt{\Big(x+\xi_x(t)\Big)^2+\Big(y-\xi_y(t)\Big)^2} + \ln\sqrt{\Big(x-\xi_x(t)\Big)^2+\Big(y-\xi_y(t)\Big)^2}\right].$$

The first term is for the image vortex and the second term is for the original vortex. The horizontal and vertical components of the induced velocity for both vortices are:

$$u(x,y,t) = \frac{\partial\psi}{\partial y} = \frac{\Gamma}{2\pi}\left[-\frac{y-\xi_y(t)}{\Big(x+\xi_x(t)\Big)^2+\Big(y-\xi_y(t)\Big)^2} + \frac{y-\xi_y(t)}{\Big(x-\xi_x(t)\Big)^2+\Big(y-\xi_y(t)\Big)^2}\right] = \frac{\partial\phi}{\partial x},$$

$$v(x,y,t) = -\frac{\partial\psi}{\partial x} = -\frac{\Gamma}{2\pi}\left[-\frac{x+\xi_x(t)}{\Big(x+\xi_x(t)\Big)^2+\Big(y-\xi_y(t)\Big)^2} + \frac{x-\xi_x(t)}{\Big(x-\xi_x(t)\Big)^2+\Big(y-\xi_y(t)\Big)^2}\right] = \frac{\partial\phi}{\partial y}.$$

As expected, the use of an opposite sign image vortex produces $u(0,y) = 0$. Free vortices move with fluid elements and follow path lines, thus:

$$\frac{d\xi_x(t)}{dt} = \lim_{\mathbf{x}\to\boldsymbol{\xi}}(u(x,y,t)), \text{ and } \frac{d\xi_y(t)}{dt} = \lim_{\mathbf{x}\to\boldsymbol{\xi}}(v(x,y,t)).$$

The equations for the velocity components given above include contributions from the image and original vortices. The limit of the image vortex's induced velocity at the location of the original vortex is well defined. The velocity induced on the original vortex by itself is not well defined, but this is a mathematical artifact of ideal vortices. Any real vortex has a finite core size, and the self-induced velocity is well defined and equal to zero on the vortex axis when the core is axisymmetric. Thus, the self-induced velocity of an ideal vortex is taken to be zero, and the path-line equations above become:

$$\frac{d\xi_x}{dt} = 0, \text{ and } \frac{d\xi_y}{dt} = \frac{\Gamma}{2\pi}\frac{1}{2\xi_x}.$$

The solution of the first path-line equation is $\xi_x = \text{const.} = h$ where the second equality follows from the initial condition. The solution of the second equation is: $\xi_y = \Gamma t/4\pi h$, where the initial condition requires the constant of integration to be zero. Therefore, the vortex trajectory is: $\boldsymbol{\xi}(t) = (h, \Gamma t/4\pi h)$.

To determine the pressure, integrate the velocity components to determine the potential:

$$\phi(x,y,t) = +\frac{\Gamma}{2\pi}\tan^{-1}\left(\frac{y-\Gamma t/4\pi h}{x+h}\right) - \frac{\Gamma}{2\pi}\tan^{-1}\left(\frac{y-\Gamma t/4\pi h}{x-h}\right).$$

The fluid far from the vortex is quiescent so the appropriate Bernoulli equation is:

$$\frac{\partial\phi}{\partial t}+\frac{1}{2}|\nabla\phi|^2+\frac{p}{\rho}=const.=\frac{p_\infty}{\rho}$$

[(4.83) with $g=0$], where the second equality follows from evaluating the constant far from the vortex. Thus, at $x=y=0$:

$$\frac{p(0,0,t)-p_\infty}{\rho}=-\left(\frac{\partial\phi}{\partial t}+\frac{1}{2}(u^2+v^2)\right)_{x=y=0}$$

Here,

$$\left(\frac{\partial\phi}{\partial t}\right)_{x=y=0}=\frac{-\Gamma^2}{4\pi^2}\left(\frac{1}{h^2+(\Gamma t/4\pi h)^2}\right),\ u(0.0,t)=0,\ \text{and}\ v(0,0,t)=\frac{\Gamma h}{\pi}\left(\frac{1}{h^2+(\Gamma t/4\pi h)^2}\right),$$

so

$$\frac{p(0,0,t)-p_\infty}{\rho}=\frac{\Gamma^2}{4\pi^2}\left(\frac{1}{h^2+(\Gamma t/4\pi h)^2}\right)-\frac{\Gamma^2h^2}{2\pi^2}\left(\frac{1}{h^2+(\Gamma t/4\pi h)^2}\right)^2=\frac{\Gamma^2}{4\pi^2}\frac{(\Gamma t/4\pi h)^2-h^2}{\left((\Gamma t/4\pi h)^2+h^2\right)^2}.$$

6.4. COMPLEX POTENTIAL

Using complex variables and complex functions, the developments for ψ and ϕ provided in the prior two sections can be recast in terms of a single complex potential $w(z)$,

$$w\equiv\phi+i\psi, \tag{6.42}$$

where z is a complex variable:

$$z\equiv x+iy=re^{i\theta}, \tag{6.43}$$

$i=\sqrt{-1}$ is the imaginary root, (x,y) are plane Cartesian coordinates, and (r,θ) are plane polar coordinates. There are many fine texts, such as Churchill et al. (1974) or Carrier et al. (1966), that cover the relevant mathematics of complex analysis, so it is merely alluded to here. In its Cartesian form, the complex number z represents a point in the x,y-plane with x increasing on the real axis and y increasing on the imaginary axis (Figure 6.17). In its polar form, z represents the position vector $\mathbf{Oz}$, with magnitude $r=(x^2+y^2)^{1/2}$ and angle with respect to the x-axis of $\theta=\tan^{-1}(y/x)$.

The complex function $w(z)$ is *analytic* and has a unique derivative dw/dz independent of the direction of differentiation within the complex z-plane. This condition leads to the *Cauchy-Riemann conditions*:

$$\frac{\partial\phi}{\partial x}=\frac{\partial\psi}{\partial y},\ \text{and}\ \frac{\partial\phi}{\partial y}=-\frac{\partial\psi}{\partial x} \tag{6.44}$$

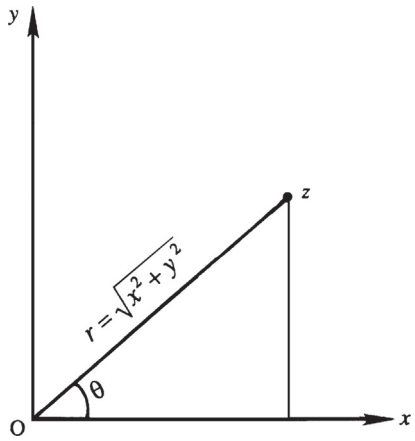

FIGURE 6.17 The complex plane where $z = x + iy = re^{i\theta}$ is the independent complex variable, $i = \sqrt{-1}$, $r = (x^2 + y^2)^{1/2}$, and $\tan\theta = y/x$.

where derivatives of $w(z)$ in the x- and iy-directions are computed separately and then equated. These equations imply that lines of constant ϕ and ψ are orthogonal. Points in the z-plane where w or dw/dz is zero or infinite are called *singularities* and at these points this orthogonality is lost.

If ϕ is interpreted as the velocity potential and ψ as the stream function, then w is the *complex potential* for the flow and (6.44) ensures the equality of the u,v-velocity components. Here, the *complex velocity* can be determined from

$$dw/dz = u - iv. \tag{6.45}$$

Applying the *Cauchy-Riemann conditions* to the complex velocity in (6.45) leads to the conditions for incompressible (6.2) and irrotational (6.9) flow, and Laplace equations for ϕ and ψ, (6.5) and (6.12), respectively. Thus, any twice-differentiable complex function of $z = x + iy$ produces solutions to Laplace's equation in the (x,y)-plane, a genuinely remarkable result! In general, a function of the two variables (x,y) may be written as $f(z, z^*)$ where $z^* = x - iy$ is the complex conjugate of z. Thus, it is the special case when $f(z, z^*) = w(z)$ alone that is considered here.

With these formal mathematical results, the correspondence between $w(z)$ and the prior results for ψ and ϕ are summarized in this and the following short paragraphs. The complex potential for flow in a corner of angle $\alpha = \pi/n$ is obtained from a power law in z,

$$w(z) = Az^n = A(re^{i\theta})^n = Ar^n(\cos n\theta + i \sin n\theta) \text{ for } n \geq 1/2, \tag{6.46}$$

where A is a real constant. When $n = 2$, the streamline pattern, $\psi = \mathrm{Im}\{w\} = Ar^2\sin 2\theta$, represents flow in a region bounded by perpendicular walls, and (6.24) and (6.27) are readily recovered from (6.46). By including the field within the second quadrant of the z-plane, it is clear that $n = 2$ also represents the flow impinging against a flat wall (Figure 6.3). The streamlines and equipotential lines are all rectangular hyperbolas. This is called a *stagnation flow* because it includes a stagnation point. For comparison, the streamline pattern for $n = 1/2$

corresponds to flow around a semi-infinite plate. In general, the complex velocity computed from (6.46) is:

$$dw/dz = nAz^{n-1} = (A\pi/\alpha)z^{(\pi-\alpha)/\alpha},$$

which shows that $dw/dz = 0$ at the origin for $\alpha < \pi$ while $dw/dz \to \infty$ at the origin for $\alpha > \pi$. Thus, in this flow the origin is a stagnation point for flow in a wall angle smaller than 180°; in contrast, it is a point of infinite velocity for wall angles larger than 180°. In both cases it is a singular point.

The complex potential for an irrotational vortex of strength Γ at (x', y'), the equivalent of (6.8), is:

$$w(z) = -\frac{i\Gamma}{2\pi}\ln(z - z') = \frac{\Gamma}{2\pi}\theta' - i\frac{\Gamma}{2\pi}\ln r', \tag{6.47}$$

where $z' = x' + iy'$, $r' = \sqrt{(x-x')^2+(y-y')^2}$, and $\theta' = \tan^{-1}((y-y')/(x-x'))$.

The complex potential for a source or sink of volume flow rate m per unit depth located at (x', y'), the equivalent of (6.15), is:

$$w(z) = \frac{m}{2\pi}\ln(z - z') = \frac{m}{2\pi}\ln(r'e^{i\theta'}) = \frac{m}{2\pi}\ln r' + i\frac{m\theta'}{2\pi}. \tag{6.48}$$

The complex potential for a doublet with dipole strength $-d\mathbf{e}_x$ located at (x', y'), the equivalent of (6.29), is:

$$w = \frac{d}{2\pi(z - z')}. \tag{6.49}$$

The complex potential for uniform flow at speed U past a half body—see (6.29), (6.30), and Figure 6.7—is the combination of a source of strength m at the origin and a uniform horizontal stream,

$$w(z) = Uz + \frac{m}{2\pi}\ln z. \tag{6.50}$$

The complex potential for uniform flow at speed U past a circular cylinder, see (6.33) and Figure 6.9, is the combination of a doublet with dipole strength $\mathbf{d} = -2\pi Ua^2\mathbf{e}_x$ and a uniform stream:

$$w = U\left(z + \frac{a^2}{z}\right). \tag{6.51}$$

When *clockwise* circulation Γ is added to the cylinder, the complex potential becomes

$$w = U\left(z + \frac{a^2}{z}\right) + \frac{i\Gamma}{2\pi}\ln(z/a), \tag{6.52}$$

the flow field is altered (see Figure 6.12), and the cylinder experiences a lift force. Here, the imaginary part of (6.52) reproduces (6.36).

The method of images also applies to the complex potential. For example, the complex potential for the flow described by (6.41) is:

$$w = \frac{m}{2\pi}\ln\left(\frac{z-a}{a}\right)+\frac{m}{2\pi}\ln\left(\frac{z+a}{a}\right)=\frac{m}{2\pi}\ln\left(\frac{z^2-a^2}{a^2}\right)=\frac{m}{2\pi}\ln\left(\frac{x^2-y^2-a^2+2ixy}{a^2}\right). \quad (6.53)$$

The complex variable description of ideal flow also allows some very general results to be obtained for pressure forces (per unit depth perpendicular to the plane of the flow) that act on two-dimensional bodies.

6.5. FORCES ON A TWO-DIMENSIONAL BODY

In Section 3 we demonstrated that the drag on a circular cylinder in steady flow is zero while the lift equals $L = \rho U\Gamma$ when the circulation is clockwise. These results are also valid for any object with an *arbitrary* noncircular cross section that does not vary in the z-direction.

Blasius Theorem

Consider a stationary object of this type with extent B perpendicular to the plane of the flow, and let D (drag) be the stream-wise (x) force component and L (lift) be cross-stream or lateral (y) force (per unit depth) exerted on the object by the surrounding fluid. Thus, from Newton's third law, the total force applied to the fluid by the object is $\mathbf{F} = -B(D\mathbf{e}_x + L\mathbf{e}_y)$. For steady irrotational constant-density flow, conservation of momentum (4.17) within a stationary control volume implies:

$$\int_{A^*} \rho\mathbf{u}(\mathbf{u}\cdot\mathbf{n})dA = -\int_{A^*} p\mathbf{n}dA + \mathbf{F}. \quad (6.54)$$

If the control surface A^* is chosen to coincide with the body surface and the body is not moving, then $\mathbf{u}\cdot\mathbf{n} = 0$ and the flux integral on the left in (6.54) is zero, so

$$D\mathbf{e}_x + L\mathbf{e}_y = -\frac{1}{B}\int_{A*} p\mathbf{n}dA. \quad (6.55)$$

If C is the contour of the body's cross section, then $dA = Bds$ where $d\mathbf{s} = \mathbf{e}_x dx + \mathbf{e}_y dy$ is an element of C and $ds = [(dx)^2 + (dy)^2]^{1/2}$. By definition, $\mathbf{n}$ must have unit magnitude, must be perpendicular to $d\mathbf{s}$, and must point outward from the control volume, so $\mathbf{n} = (\mathbf{e}_x dy - \mathbf{e}_y dx)/ds$. Using these relationships for $\mathbf{n}$ and dA, (6.55) can be separated into force components,

$$D\mathbf{e}_x + L\mathbf{e}_y = -\frac{1}{B}\oint_C p\frac{(\mathbf{e}_x dy - \mathbf{e}_y dx)}{ds}Bds = \left(-\oint_C pdy\right)\mathbf{e}_x + \left(\oint_C pdx\right)\mathbf{e}_y, \quad (6.56)$$

to identify the contour integrals leading to D and L. Here, C must be traversed in the counterclockwise direction.

Now switch from the physical domain to the complex z-plane to make use of the complex potential. This switch is accomplished here by replacing $d\mathbf{s}$ with $dz = dx + idy$ and exploiting

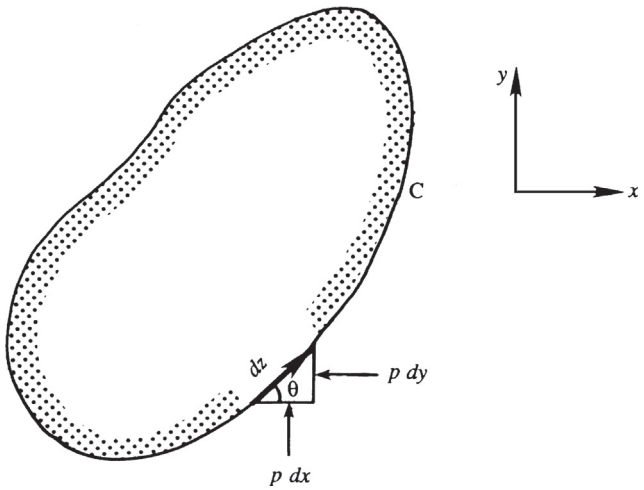

FIGURE 6.18 Elemental forces in a plane on two-dimensional object. Here the elemental horizontal and vertical force components (per unit depth) are $-pdy$ and $+pdx$, respectively.

the dichotomy between real and imaginary parts to keep track of horizontal and vertical components (see Figure 6.18). To achieve the desired final result, construct the complex force,

$$D - iL = \left(-\oint_C p dy\right) - i\left(\oint_C p dx\right) = -i\oint_C p(dx - idy) = -i\oint_C p\, dz^*, \tag{6.57}$$

where * denotes a complex conjugate. The pressure p is found from the Bernoulli equation (6.18),

$$p_\infty + \tfrac{1}{2}\rho U^2 = p + \tfrac{1}{2}\rho\left(u^2 + v^2\right) = p + \tfrac{1}{2}\rho(u - iv)(u + iv),$$

where p_∞ and U are the pressure and horizontal flow speed far from the body. Inserting this into (6.57) produces:

$$D - iL = -i\oint_C \left[p_\infty + \tfrac{1}{2}\rho U^2 - \tfrac{1}{2}\rho(u - iv)(u + iv)\right] dz^*. \tag{6.58}$$

The integral of the constant terms, $p_\infty + \rho U^2/2$, around a closed contour is zero. The body-surface velocity vector and the surface element $dz = |dz|e^{i\theta}$ are parallel, so $(u + iv)dz^*$ can be rewritten

$$(u + iv)dz^* = \left[u^2 + v^2\right]^{1/2} e^{i\theta}|dz|e^{-i\theta} = \left[u^2 + v^2\right]^{1/2} e^{-i\theta}|dz|e^{i\theta} = (u - iv)dz = (dw/dz)dz, \tag{6.59}$$

where (6.45) has been used for the final equality. Thus, (6.58) reduces to

$$D - iL = \frac{i\rho}{2}\oint_C \left(\frac{dw}{dz}\right)^2 dz, \tag{6.60}$$

a result known as the *Blasius theorem*. It applies to any plane steady ideal flow. Interestingly, the integral need not be carried out along the contour of the body because the theory of complex variables allows *any contour surrounding the body to be chosen* provided there are no singularities in $(dw/dz)^2$ between the body and the contour chosen.

Kutta–Zhukhovsky Lift Theorem

The Blasius theorem can be readily applied to an arbitrary cross-section object around which there is circulation $-\Gamma$. The flow can be considered a superposition of a uniform stream and a set of singularities such as vortex, doublet, source, and sink.

As there are no singularities outside the body, we shall take the contour C in the Blasius theorem at a very large distance from the body. From large distances, all singularities appear to be located near the origin $z = 0$, so the complex potential on the contour C will be of the form:

$$w = Uz + \frac{m}{2\pi}\ln z + \frac{i\Gamma}{2\pi}\ln z + \frac{d}{2\pi z} + \ldots$$

When U, m, Γ, and d are positive and real, the first term represents a uniform flow in the x-direction, the second term represents a net source of fluid, the third term represents a clockwise vortex, and the fourth term represents a doublet. Because the body contour is closed, there can be no net flux of fluid into the domain. The sinks must scavenge all the flow introduced by the sources, so $m = 0$. The Blasius theorem, (6.60), then becomes

$$D - iL = \frac{i\rho}{2}\oint_C \left(U + \frac{i\Gamma}{2\pi z} - \frac{d}{2\pi z^2} + \ldots\right)^2 dz = \frac{i\rho}{2}\oint_C \left(U^2 + \frac{iU\Gamma}{\pi}\frac{1}{z} + \left(\frac{Ud}{\pi} - \frac{\Gamma^2}{4\pi^2}\right)\frac{1}{z^2} + \ldots\right)dz. \tag{6.61}$$

To evaluate the contour integral in (6.61), we simply have to find the coefficient of the term proportional to $1/z$ in the integrand. This coefficient is known as the *residue* at $z = 0$ and the residue theorem of complex variable theory states that the value of a contour integral like (6.61) is $2\pi i$ times the sum of the residues at all singularities inside C. Here, the only singularity is at $z = 0$, and its residue is $iU\Gamma/\pi$, so

$$D - iL = \frac{i\rho}{2}2\pi i\left(\frac{iU\Gamma}{\pi}\right) = -i\rho U\Gamma \text{ or } D = 0 \text{ and } L = \rho U\Gamma. \tag{6.62}$$

Thus, there is no drag on an arbitrary-cross-section object in steady two-dimensional, irrotational constant-density flow, a more general statement of d'Alembert's paradox. Given that nonzero drag forces are an omnipresent fact of everyday life, this might seem to eliminate any practical utility for ideal flow. However, there are at least three reasons to avoid this presumption. First of all, ideal flow streamlines indicate what a real flow should look like to achieve minimum pressure drag. Lower drag on real objects is often realized when object-geometry changes are made or boundary-layer, separation-control strategies are implemented that allow real-flow streamlines to better match their ideal-flow counterparts. Second, the predicted circulation-dependent force on the object perpendicular to the oncoming stream—the lift force, $L = \rho U\Gamma$—is basically correct. The result (6.62) is called

the *Kutta-Zhukhovsky lift theorem*, and it plays a fundamental role in aero- and hydrodynamics. As described in Chapter 14, the circulation developed by an air- or hydrofoil is nearly proportional to U, so L is nearly proportional to U^2. And third, the influence of viscosity in real fluid flows takes some time to develop, so impulsively started flows and rapidly oscillating flows (i.e., acoustic fluctuations) often follow ideal flow streamlines.

6.6. CONFORMAL MAPPING

We shall now introduce a method by which complex flow patterns can be transformed into simple ones using a technique known as *conformal mapping* in complex variable theory. Consider the functional relationship $w = f(z)$, which maps a point in the w-plane to a point in the z-plane, and vice versa. We shall prove that infinitesimal figures in the two planes preserve their geometric similarity if $w = f(z)$ is analytic. Let lines C_z and C_z' in the z-plane be transformations of the curves C_w and C_w' in the w-plane, respectively (Figure 6.19). Let δz, $\delta' z$, δw, and $\delta' w$ be infinitesimal elements along the curves as shown. The four elements are related by

$$\delta w = \frac{dw}{dz}\delta z, \tag{6.63}$$

$$\delta' w = \frac{dw}{dz}\delta' z. \tag{6.64}$$

If $w = f(z)$ is analytic, then dw/dz is independent of orientation of the elements, and therefore has the same value in (6.63) and (6.64). These two equations then imply that the elements δz and $\delta' z$ are rotated by the *same amount* (equal to the argument of dw/dz) to obtain the elements δw and $\delta' w$. It follows that

$$\alpha = \beta,$$

which demonstrates that infinitesimal figures in the two planes are geometrically similar. The demonstration fails at singular points at which dw/dz is either zero or infinite. Because dw/dz is a function of z, the amount of magnification and rotation that an element δz undergoes during transformation from the z-plane to the w-plane varies. Consequently, *large* figures become distorted during the transformation.

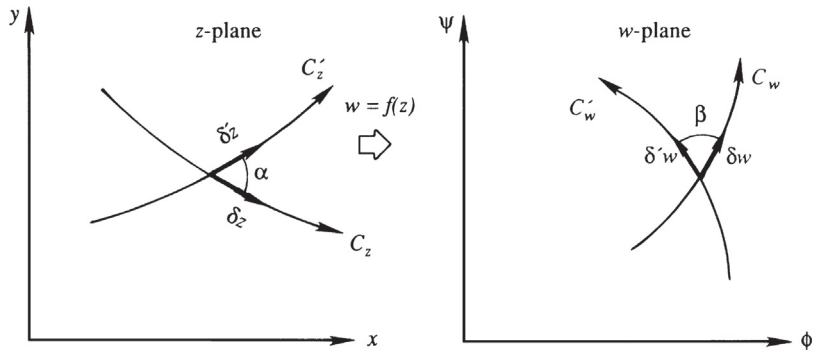

FIGURE 6.19 Preservation of geometric similarity of small elements in conformal mapping between the complex z- and w-planes.

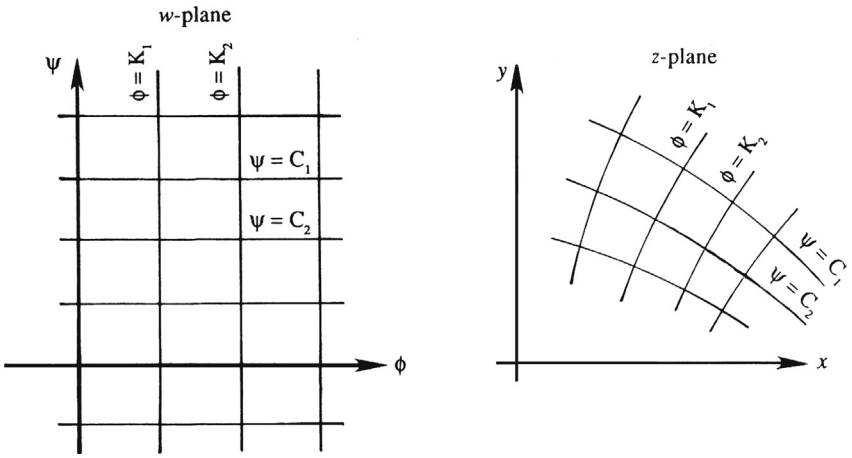

FIGURE 6.20 Flow patterns in the complex w-plane and the z-plane. The w-plane represents uniform flow with straight potential lines and streamlines. In the z-plane these lines curve to represent the flow of interest.

In application of conformal mapping, we always choose a rectangular grid in the w-plane consisting of constant ϕ and ψ lines (Figure 6.20). In other words, we define ϕ and ψ to be the real and imaginary parts of w:

$$w = \phi + i\psi.$$

The rectangular net in the w-plane represents a uniform flow in this plane. The constant ϕ and ψ lines are transformed into certain curves in the z-plane through the transformation $w = f(z)$ or its inverse $f^{-1}(w) = z$. *The pattern in the z-plane is the physical pattern under investigation*, and the images of constant ϕ and ψ lines in the z-plane form the equipotential lines and streamlines, respectively, of the desired flow. We say that $w = f(z)$ transforms a uniform flow in the w-plane into the desired flow in the z-plane. In fact, all the preceding flow patterns studied through the transformation $w = f(z)$ can be interpreted this way.

If the physical pattern under investigation is too complicated, we may introduce intermediate transformations in going from the w-plane to the z-plane. For example, the transformation $w = \ln(\sin z)$ can be broken into

$$w = \ln\zeta \qquad \zeta = \sin z.$$

Velocity components in the z-plane are given by

$$u - iv = \frac{dw}{dz} = \frac{dw}{d\zeta}\frac{d\zeta}{dz} = \frac{1}{\zeta}\cos z = \cot z.$$

As a simple example of conformal mapping, consider the transformation, $w = \phi + i\psi = z^2 = x^2 + y^2 + 2ixy$. Streamlines are given by $\psi = const = 2xy$, rectangular hyperbolae (see Figure 6.5). Here uniform flow in the w-plane has been mapped onto flow in a 90° corner in the z-plane by this transformation. A more involved example follows. Additional applications are discussed in Chapter 14.

The Zhukhovsky transformation relates two complex variables z and ζ, and has important applications in airfoil theory,

$$z = \zeta + \frac{b^2}{\zeta}. \tag{6.65}$$

When $|\zeta|$ or $|z|$ is very large compared to b, this transformation becomes an identity, so it does not change the flow condition far from the origin when moving between the z and ζ planes. However, close to the origin, (6.65) transforms a circle of radius b centered at the origin of the ζ-plane into a line segment on the real axis of the z-plane. To establish this, let $\zeta = b\exp(i\theta)$ on the circle (Figure 6.21) so that (6.65) provides the corresponding point in the z-plane as:

$$z = be^{i\theta} + be^{-i\theta} = 2b\cos\theta.$$

As θ varies from 0 to π, z goes along the x-axis from $2b$ to $-2b$. As θ varies from π to 2π, z goes from $-2b$ to $2b$. The circle of radius b in the ζ-plane is thus transformed into a line segment of length $4b$ in the z-plane. The region *outside* the circle in the ζ-plane is mapped into the *entire* z-plane. It can be shown that the region inside the circle is also transformed into the entire z-plane. This, however, is of no concern to us because we shall not consider the interior of the circle in the ζ-plane.

Now consider a circle of radius $a > b$ in the ζ-plane (Figure 6.21). A point $\zeta = a\exp(i\theta)$ on this circle is transformed to

$$z = ae^{i\theta} + \frac{b^2}{a}e^{-i\theta}, \tag{6.66}$$

which traces out an ellipse for various values of θ; the geometry becomes clear by separating real and imaginary parts of (6.66) and eliminating θ:

$$\frac{x^2}{(a + b^2/a)^2} + \frac{y^2}{(a - b^2/a)^2} = 1. \tag{6.67}$$

For various values of $a > b$, (6.67) represents a family of ellipses in the z-plane, with foci at $x = \pm 2b$.

The flow around one of these ellipses (in the z-plane) can be determined by first finding the flow around a circle of radius a in the ζ-plane, and then using (6.65) to go to the z-plane.

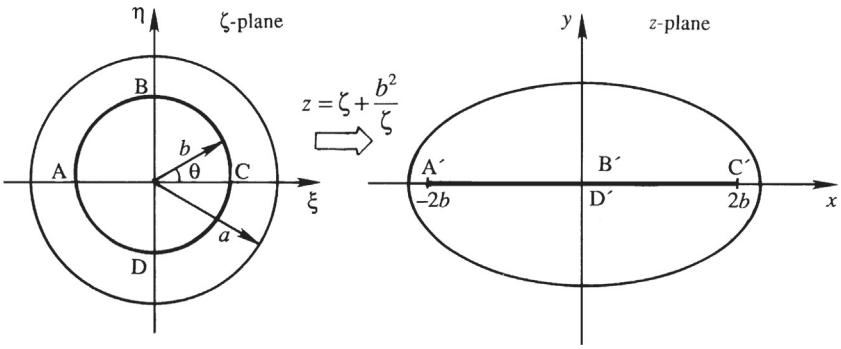

FIGURE 6.21 Transformation of a circle of radius a in the ζ-plane into an ellipse in the z-plane by means of the Zhukhovsky transformation $z = \zeta + b^2/\zeta$. A circle of radius b in the ζ-plane transforms into a line segment between $z = \pm 2b$ in the z-plane.

To be specific, suppose the desired flow in the z-plane is that of flow around an elliptic cylinder with clockwise circulation Γ placed in a stream moving at U. The corresponding flow in the ζ-plane is that of flow with the same circulation around a circular cylinder of radius a placed in a horizontal stream of speed U. The complex potential for this flow is (6.52) with z replaced by ζ:

$$w = U\left(\zeta + \frac{a^2}{\zeta}\right) + \frac{i\Gamma}{2\pi}\ln(\zeta/a). \tag{6.68}$$

The complex potential $w(z)$ in the z-plane can be found by substituting the inverse of (6.65),

$$\zeta = \frac{1}{2}z + \frac{1}{2}\left(z^2 - 4b^2\right)^{1/2}, \tag{6.69}$$

into (6.68). Here, the negative root, which falls inside the cylinder, has been excluded from (6.69). Instead of finding the complex velocity in the z-plane by directly differentiating $w(z)$, it is easier to find it as

$$u - iv = \frac{dw}{dz} = \frac{dw}{d\zeta}\frac{d\zeta}{dz}.$$

The resulting flow around an elliptic cylinder with circulation is qualitatively quite similar to that around a circular cylinder as shown in Figure 6.12.

6.7. NUMERICAL SOLUTION TECHNIQUES IN TWO DIMENSIONS

Exact solutions can be obtained only for flows with relatively simple geometries, so approximate methods of solution become necessary for complicated geometries. One of these approximate methods is that of building up a flow by superposing a distribution of sources and sinks; this method is illustrated in Section 6.8 for axisymmetric flows. Another method is to apply perturbation techniques by assuming that the body is thin. A third method is to solve the Laplace equation numerically. In this section we shall illustrate the numerical method in its simplest form without worrying about computational efficiency. It is hoped that the reader will have an opportunity to learn numerical methods that are becoming increasingly important in the applied sciences in a separate study. Introductory material on several important techniques of computational fluid dynamics is provided in Chapter 10.

Numerical techniques for solving the Laplace equation typically rely on discretizing the spatial domain. When using finite difference techniques, the flow field is discretized into a system of *grid points*, and field derivatives are computed by taking differences between field values at adjacent grid points. Let the coordinates of a point be represented by

$$x = i\Delta x (i = 0, 1, 2, \ldots), \text{ and } y = j\Delta y (j = 0, 1, 2, \ldots).$$

Here, Δx and Δy are the dimensions of a grid cell, and the integers i and j are the indices associated with a grid point (Figure 6.22). The stream function $\psi(x,y)$ can be represented at these discrete locations by

$$\psi(x, y) = \psi\left(i\,\Delta x, j\,\Delta y\right) \equiv \psi_{i,j},$$

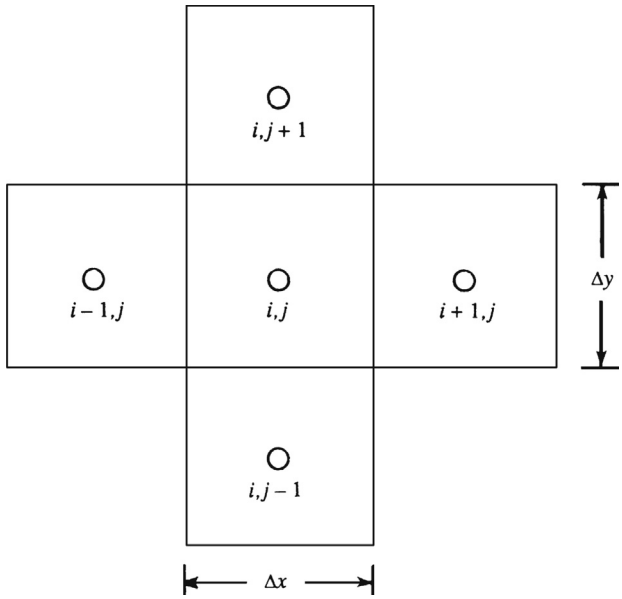

FIGURE 6.22 Adjacent grid boxes in a numerical calculation showing how the indices i and j change.

where $\psi_{i,j}$ is the value of ψ at the grid point (i, j) (the comma notation for derivatives is not applied here). In finite difference form, the first derivatives of ψ_i are approximated as first-order central differences:

$$\left(\frac{\partial\psi}{\partial x}\right)_{i,j} \simeq \frac{1}{\Delta x}\left(\psi_{i+\frac{1}{2},j} - \psi_{i-\frac{1}{2},j}\right), \text{ and } \left(\frac{\partial\psi}{\partial y}\right)_{i,j} \simeq \frac{1}{\Delta y}\left(\psi_{i,j+\frac{1}{2}} - \psi_{i,j-\frac{1}{2}}\right).$$

The quantities on the right side of each equation (such as $\psi_{i+1/2,j}$) are halfway between the grid points and therefore undefined. However, this potential difficulty is avoided here because the Laplace equation does not involve first derivatives. Applying the same approach to the second-order x-derivative produces:

$$\begin{aligned}\left(\frac{\partial^2\psi}{\partial x^2}\right)_{i,j} &\simeq \frac{1}{\Delta x}\left[\left(\frac{\partial\psi}{\partial x}\right)_{i+\frac{1}{2},j} - \left(\frac{\partial\psi}{\partial x}\right)_{i-\frac{1}{2},j}\right], \\ &\simeq \frac{1}{\Delta x}\left[\frac{1}{\Delta x}\left(\psi_{i+1,j} - \psi_{i,j}\right) - \frac{1}{\Delta x}\left(\psi_{i,j} - \psi_{i-1,j}\right)\right], \\ &= \frac{1}{\Delta x^2}\left[\psi_{i+1,j} - 2\psi_{i,j} + \psi_{i-1,j}\right].\end{aligned} \tag{6.70}$$

Similarly,

$$\left(\frac{\partial^2\psi}{\partial y^2}\right)_{i,j} \simeq \frac{1}{\Delta y^2}\left[\psi_{i,j+1} - 2\psi_{i,j} + \psi_{i,j-1}\right]. \tag{6.71}$$

Using (6.70) and (6.71), the Laplace equation (6.5) for the stream function in a plane two-dimensional flow has a finite difference representation:

$$\frac{1}{\Delta x^2}\left[\psi_{i+1,j} - 2\psi_{i,j} + \psi_{i-1,j}\right] + \frac{1}{\Delta y^2}\left[\psi_{i,j+1} - 2\psi_{i,j} + \psi_{i,j-1}\right] = 0.$$

Taking $\Delta x = \Delta y$, for simplicity, this reduces to

$$\psi_{i,j} = \frac{1}{4}\left[\psi_{i-1,j} + \psi_{i+1,j} + \psi_{i,j-1} + \psi_{i,j+1}\right], \tag{6.72}$$

which shows that ψ satisfies the Laplace equation if its value at a grid point equals the average of the values at the four surrounding points.

Equation (6.72) can be solved by a simple iteration technique when the values of ψ are given on the boundary. First consider a readily countable number of grid points covering the rectangular region of Figure 6.23 where the flow field is discretized with 16 grid points with $1 \leq i, j \leq 4$. Of these, the values of ψ are presumed known at the 12 boundary points indicated by open circles. The values of ψ at the four interior points indicated by solid circles are unknown. For these interior points, (6.72) gives

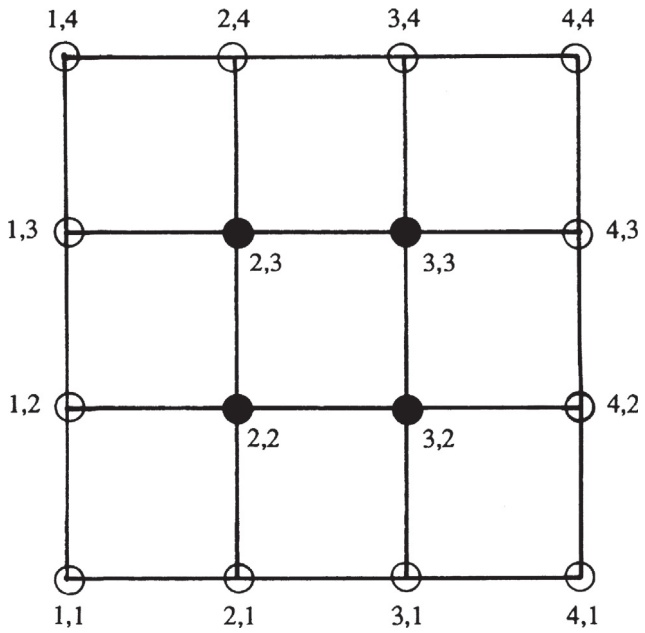

FIGURE 6.23 Network of sixteen grid points arrayed in a rectangular grid. The *i,j*-values at each point are listed. Boundary points with known values are indicated by open circles. The four interior points with unknown values are indicated by solid circles.

$$\begin{aligned}
\psi_{2,2} &= \frac{1}{4}\Big[\psi^B_{1,2} + \psi_{3,2} + \psi^B_{2,1} + \psi_{2,3}\Big],\\
\psi_{3,2} &= \frac{1}{4}\Big[\psi_{2,2} + \psi^B_{4,2} + \psi^B_{3,1} + \psi_{3,3}\Big],\\
\psi_{2,3} &= \frac{1}{4}\Big[\psi^B_{1,3} + \psi_{3,3} + \psi_{2,2} + \psi^B_{2,4}\Big],\\
\psi_{3,3} &= \frac{1}{4}\Big[\psi_{2,3} + \psi^B_{4,3} + \psi_{3,2} + \psi^B_{3,4}\Big].
\end{aligned} \tag{6.73}$$

Here, the known boundary values have been indicated by a superscript "B." The equation set (6.73) represents four linear algebraic equations in four unknowns and is therefore solvable.

In practice, however, a much larger number of grid points will likely be used to represent the flow field, and a computer will determine a numerical solution of the resulting large number of simultaneous algebraic equations. One of the simplest techniques of solving such a large equation set is the *iteration method* where an initial solution guess is gradually improved and updated until (6.73) is satisfied at every point. For example, suppose the initial guesses for ψ at the four unknown points of Figure 6.23 are all zero. From (6.73), the first estimate of $\psi_{2,2}$ can be computed as

$$\psi_{2,2} = \frac{1}{4}\Big[\psi^B_{1,2} + 0 + \psi^B_{2,1} + 0\Big].$$

The initial zero value for $\psi_{2,2}$ is now replaced by this *updated* value. The first estimate for the next grid point is then obtained as

$$\psi_{3,2} = \frac{1}{4}\Big[\psi_{2,2} + \psi^B_{4,2} + \psi^B_{3,1} + 0\Big],$$

where the updated value of $\psi_{2,2}$ has been used on the right-hand side. In this manner, we can sweep over the entire flow domain in a systematic manner, *always using the latest available value at each point*. Once the first estimate at every point has been obtained, the domain sweep can be repeated to obtain second estimates and this process can be repeated again and again until the values of $\psi_{i,j}$ do not change appreciably between two successive sweeps. At this point, the iteration process has *converged*.

The foregoing scheme is particularly suitable for implementation using a computer, where it is easy to replace old values at a point as soon as a new value is available. In practice, more sophisticated and efficient numerical techniques are used in large calculations. However, the purpose here is to present the simplest numerical solution technique, which is illustrated in the following example.

EXAMPLE 6.2

Figure 6.24 shows a contraction in a channel through which the flow rate per unit depth is 5 m^2/s. The velocity is uniform and parallel across the inlet and outlet sections. Find the stream function values within this flow field.

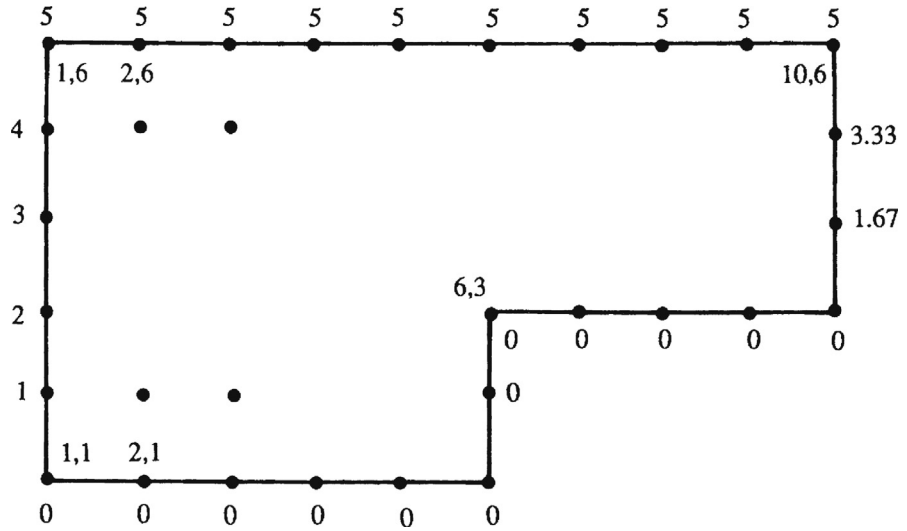

FIGURE 6.24 Grid pattern for irrotational flow through an abrupt, sharp-cornered contraction (Example 6.2). The flow enters on the left and exits on the right. The boundary values of ψ are indicated on the outside. The values of i, j for some grid points are indicated on the inside.

Solution

The region of flow is two-dimensional but is singly connected because the flow field *is interior* to the boundaries and every fluid-only circuit can be reduced to a point. Therefore, the problem has a unique solution that can be found numerically.

The difference in ψ values is equal to the flow rate between two streamlines. Thus, setting $\psi = 0$ at the bottom wall requires $\psi = 5\ \text{m}^2/\text{s}$ at the top wall. We divide the field into the system of grid points shown, with $\Delta x = \Delta y = 1$ m. Because $\Delta\psi/\Delta y\ (= u)$ is given to be uniform across the inlet and the outlet, we must have $\Delta\psi = 1\ \text{m}^2$ at the inlet and $\Delta\psi = 5/3 = 1.67\ \text{m}^2/\text{s}$ at the outlet. The resulting values of ψ at the boundary points are indicated in Figure 6.25. A FORTRAN code for solving the problem is as follows:

```
      DIMENSION S(10, 6)

         DO 10 I=1,6
   10    S(I,1)=0.
         DO 20 I=2,3
   20    S(6,J)=0.                  } Set ψ on top and bottom walls
         DO 30 I=7,10
   30    S(I,3)=0.
         DO 40 I=1,10
   40    S(I,6)=5.

         DO 50 J=2,6
   50    S(1,J) = J-1.              } Set ψ at inlet
```

```
      DO 60 J=4,6                    }
   60 S(10,J)=(J-3)*(5./3.)          } Set ψ at outlet

      DO 100 N=1,20
      DO 70 I=2,5
      DO 70 J=2,5
   70 S(I,J)=(S(I,J+1)+S(I,J-1)+S(I+1,J)+S(I-1,J))/4.
      DO 80 I=6,9
      DO 80 J=4,5
   80 S(I,J)=(S(I,J+1)+S(I,J-1)+S(I+1,J)+S(I-1,J))/4.
  100 CONTINUE
      PRINT 1, ((S(I,J),I=1,10),J=1,6)
    1 FORMAT (' ', 10 E 12.4')
      END
```

Here, S denotes the stream function ψ. The code first sets the boundary values. The iteration is performed in the N loop. In practice, iterations will not be performed arbitrarily 20 times. Instead the convergence of the iteration process will be checked, and the process is continued until some reasonable criterion (such as less than 1% change at every point) is met. However, some caution is appropriate. To be sure a numerical solution has been obtained, all the terms in the field equation must be calculated and the satisfaction of the field equation by the numerical solution must be verified. Such improvements are easy to implement, so the code above is left in its simplest form. The values of ψ at the grid points after 50 iterations, and the corresponding streamlines, are shown in Figure 6.25.

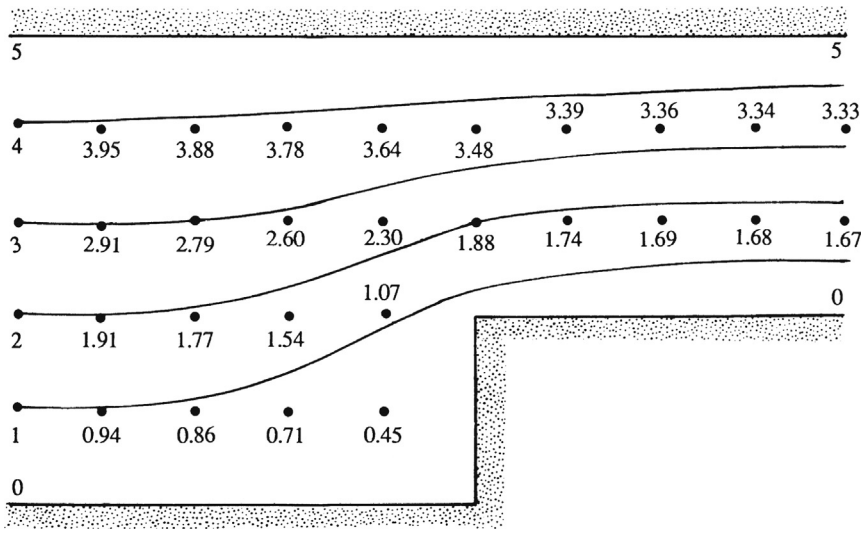

FIGURE 6.25 Numerical solution of Example 6.2 for the boundary conditions shown in Figure 6.24. The numerical values listed are for the corresponding grid points shown as black dots. Note that there is some streamline curvature after the abrupt contraction.

6.8. AXISYMMETRIC IDEAL FLOW

Two stream functions are required to describe a fully three-dimensional flow (Section 4.3). However, when the flow is axisymmetric, a single stream function can again be used. Thus, the development presented here parallels that in Section 6.2 for plane ideal flow.

In (R, φ, z) cylindrical coordinates, the axisymmetric incompressible continuity equation is:

$$\frac{1}{R}\frac{\partial}{\partial R}(Ru_R) + \frac{\partial u_z}{\partial z} = 0. \tag{6.74}$$

As discussed near the end of Section 4.3, this equation may be solved by choosing the first three-dimensional stream function $\chi = -\varphi$, so that $\mathbf{u} = (u_R,\ 0,\ u_z) = \nabla\chi \times \nabla\psi = -(1/R)\,\mathbf{e}_\varphi \times \nabla\psi$, which implies

$$u_R = -\frac{1}{R}\frac{\partial \psi}{\partial z}, \text{ and } u_z = \frac{1}{R}\frac{\partial \psi}{\partial R}. \tag{6.75}$$

Substituting these into the equation for the φ-component of vorticity,

$$\omega_\varphi = \frac{\partial u_R}{\partial z} - \frac{\partial u_z}{\partial R}, \tag{6.76}$$

produces the field equation for the axisymmetric stream function in irrotational flow:

$$\frac{\partial}{\partial R}\left(\frac{1}{R}\frac{\partial \psi}{\partial R}\right) + \frac{1}{R}\frac{\partial^2 \psi}{\partial z^2} = -\omega_\varphi = 0. \tag{6.77}$$

This *is not* the two-dimensional Laplace equation. Therefore, the complex variable formulation for plane ideal flows does not apply to axisymmetric ideal flow.

The axisymmetric stream function is sometimes called the *Stokes stream function*. It has units of m^3/s, in contrast to the plane-flow stream function, which has units of m^2/s. Surfaces of $\psi =$ constant in axisymmetric flow are surfaces of revolution. The volume flow rate dQ between two axisymmetric stream surfaces described by constant values ψ and $\psi + d\psi$ (Figure 6.26) is

$$dQ = 2\pi R(\mathbf{u}\cdot\mathbf{n})ds = 2\pi R(-u_R dz + u_z dR) = 2\pi\left(\frac{\partial \psi}{\partial z}dz + \frac{\partial \psi}{\partial R}dR\right) = 2\pi d\psi, \tag{6.78}$$

where $\mathbf{u} = u_R\mathbf{e}_R + u_z\mathbf{e}_z$, $\mathbf{n} = (-\mathbf{e}_R dz + \mathbf{e}_z dR)/ds$, and (6.75) has been used. Note that as drawn in Figure 6.26 dz is negative. The form $d\psi = dQ/2\pi$ shows that the difference in ψ values is the flow rate between two concentric stream surfaces per unit radian angle around the axis. This is consistent with the discussion of stream functions in Section 4.3. The factor of 2π is absent in plane flows, where $d\psi = dQ$ is the flow rate per unit depth perpendicular to the plane of the flow.

Here also an axisymmetric potential function ϕ can be defined via $\mathbf{u} = \nabla\phi$ or

$$u_R = \partial\phi/\partial R \text{ and } u_z = \partial\phi/\partial z, \tag{6.79}$$

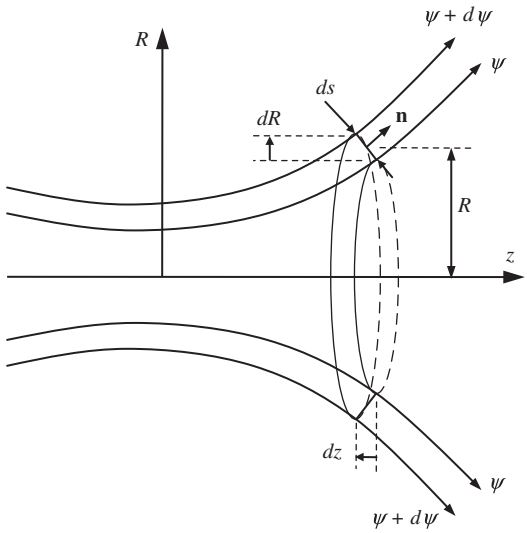

FIGURE 6.26 Geometry for calculating the volume flow rate between axisymmetric-flow stream surfaces with values of ψ and $\psi + d\psi$. The z-axis is the axis of symmetry, R is the radial distance from the z-axis, $ds = \mathbf{e}_R dR + \mathbf{e}_z dz$ is the distance between the two surfaces, and $\mathbf{n}$ is a unit vector perpendicular to ds. The volume flow rate between the two surfaces is $2\pi d\psi$.

so that the flow identically satisfies $\omega_\varphi = 0$. Substituting (6.79) into the incompressible continuity equation produces the field equation for axisymmetric potential function:

$$\frac{1}{R}\frac{\partial}{\partial R}\left(R\frac{\partial \phi}{\partial R}\right) + \frac{\partial^2 \phi}{\partial z^2} = 0. \tag{6.80}$$

While this *is* the axisymmetric Laplace equation, it is not the same as the two-dimensional Cartesian version.

In axisymmetric flow problems, both (R, φ, z)-cylindrical and (r, θ, φ)-spherical polar coordinates are commonly used. These are illustrated in Figure 3.3 with the z-axis and polar-axis vertical. The angle φ is the same in both systems. Axisymmetric flows are independent φ, and their velocity component, u_φ, in the φ direction is zero. In this section, we will commonly point the z-axis horizontal. Note that R is the radial distance from the axis of symmetry (the z-axis or polar axis) in cylindrical coordinates, whereas r is the distance from the origin in spherical coordinates. Important expressions for these curvilinear coordinates are listed in Appendix B. Several relevant expressions are provided here for easy reference.

Cylindrical	Spherical
$x = R\cos\varphi$	$x = r\sin\theta\cos\varphi$
$y = R\sin\varphi$	$y = r\sin\theta\sin\varphi$
$z = z$	$z = r\cos\theta$

(6.81)

Cylindrical	Spherical	
Continuity equations (6.74)	$\frac{1}{r}\frac{\partial}{\partial r}(r^2 u_r) + \frac{1}{\sin\theta}\frac{\partial}{\partial\theta}(u_\theta \sin\theta) = 0$	(6.82)
Velocity components (6.75), (6.79)	$u_r = \frac{1}{r^2 \sin\theta}\frac{\partial\psi}{\partial\theta} = \frac{\partial\phi}{\partial r},\ u_\theta = -\frac{1}{r\sin\theta}\frac{\partial\psi}{\partial r} = \frac{1}{r}\frac{\partial\phi}{\partial\theta}$	(6.83)
Vorticity (6.76)	$\omega_\varphi = \frac{1}{r}\left[\frac{\partial}{\partial r}(ru_\theta) - \frac{\partial u_r}{\partial\theta}\right]$	(6.84)
Laplace equation (6.80)	$\frac{1}{r^2}\frac{\partial}{\partial r}\left(r^2\frac{\partial\phi}{\partial r}\right) + \frac{1}{r^2\sin\theta}\frac{\partial}{\partial\theta}\left(\sin\theta\frac{\partial\phi}{\partial\theta}\right) = 0$	(6.85)

Some simple examples of axisymmetric irrotational flows around bodies of revolution, such as spheres and airships, are provided in the rest of this section.

Axisymmetric ideal flows can be constructed from elementary solutions in the same manner as plane flows, except that complex variables cannot be used. Several elementary flows are tabulated here

Cylindrical	Spherical	
Uniform flow in the z direction		
$\phi = Uz,\ \psi = \frac{1}{2}UR^2$	$\phi = Ur\cos\theta,\ \psi = \frac{1}{2}Ur^2\sin^2\theta$	(6.86)
Point source of strength $Q(\mathrm{m}^3/\mathrm{s})$ *at the origin of coordinates*		
$\phi = \frac{-Q}{4\pi\sqrt{R^2+z^2}},\ \psi = \frac{-Qz}{4\pi\sqrt{R^2+z^2}}$	$\phi = -\frac{Q}{4\pi r},\ \psi = -\frac{Q}{4\pi}\cos\theta$	(6.87)
Doublet with dipole strength $-d\mathbf{e}_z$ *at the origin of coordinates*		
$\phi = \frac{d}{4\pi}\frac{z}{(R^2+z^2)^{3/2}},\ \psi = -\frac{d}{4\pi}\frac{R^2}{(R^2+z^2)^{3/2}}$	$\phi = \frac{d}{4\pi r^2}\cos\theta,\ \psi = -\frac{d}{4\pi r}\sin^2\theta$	(6.88)

For these three flows, streamlines in any plane containing the axis of symmetry will be qualitatively similar to those of their two-dimensional counterparts.

Potential flow around a sphere can be generated by the superposition of a uniform stream $U\mathbf{e}_z$ and an axisymmetric doublet opposing the stream of strength $d = 2\pi a^3 U$. In spherical coordinates, the stream and potential functions are:

$$\begin{aligned}\psi &= \frac{1}{2}Ur^2\sin^2\theta - \frac{d}{4\pi r}\sin^2\theta = \frac{1}{2}Ur^2\left(1-\frac{a^3}{r^3}\right)\sin^2\theta;\\ \phi &= Ur\cos\theta + \frac{d}{4\pi r^2}\cos\theta = Ur\left(1+\frac{a^3}{2r^3}\right)\cos\theta.\end{aligned} \tag{6.89}$$

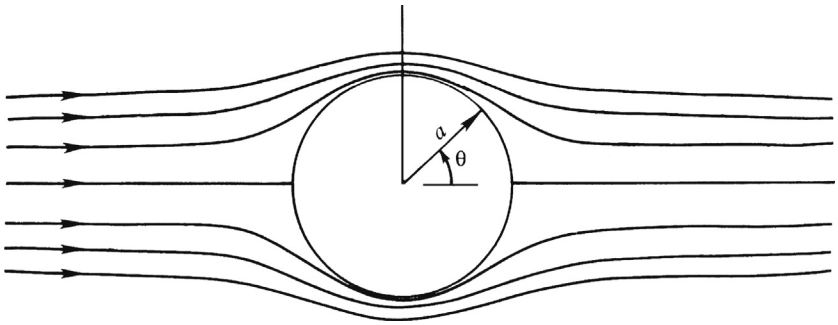

FIGURE 6.27 Axisymmetric streamlines for ideal flow past a sphere in a plane containing the axis of symmetry. The flow is fastest and the streamlines are closest together at $\theta = 90°$. The streamlines upstream and downstream of the sphere are the same, so there is no drag on the sphere.

This shows that $\psi = 0$ for $\theta = 0$ or π (for any $r \neq 0$), or for $r = a$ (for any θ). Thus the entire z-axis and the spherical surface of radius a form the stream surface $\psi = 0$. Streamlines for this flow are shown in Figure 6.27. The velocity components are:

$$\begin{aligned} u_r &= \frac{1}{r^2 \sin\theta}\frac{\partial\psi}{\partial\theta} = U\left[1 - \left(\frac{a}{r}\right)^3\right]\cos\theta, \\ u_\theta &= -\frac{1}{r\sin\theta}\frac{\partial\psi}{\partial r} = -U\left[1 + \frac{1}{2}\left(\frac{a}{r}\right)^3\right]\sin\theta. \end{aligned} \tag{6.90}$$

The pressure coefficient on the sphere's surface is

$$C_p = \frac{p - p_\infty}{\frac{1}{2}\rho U^2} = 1 - \left(\frac{u_\theta}{U}\right)^2 = 1 - \frac{9}{4}\sin^2\theta, \tag{6.91}$$

which is fore-aft symmetrical, again demonstrating zero drag in steady ideal flow.

Interestingly, the potential for this flow can be rewritten to eliminate the dependence on the coordinate system. Start from the first equality for the potential in (6.89) and use $\mathbf{x} = r\mathbf{e}_r$, $|\mathbf{x}| = r$, $\cos\theta = \mathbf{e}_z \cdot \mathbf{e}_r$, $\mathbf{U} = U\mathbf{e}_z$, and $\mathbf{d} = -d\mathbf{e}_z$, to find:

$$\begin{aligned} \phi &= Ur\cos\theta + \frac{d}{4\pi r^2}\cos\theta = U\mathbf{e}_z \cdot r\mathbf{e}_r - \frac{\mathbf{d}}{4\pi r^3}\cdot r\mathbf{e}_r \\ &= \mathbf{U}\cdot\mathbf{x} - \frac{\mathbf{d}}{4\pi|\mathbf{x}|^3}\cdot\mathbf{x} = \left(\mathbf{U} - \frac{\mathbf{d}}{4\pi|\mathbf{x}|^3}\right)\cdot\mathbf{x}, \end{aligned} \tag{6.92}$$

a result that will be useful in the next section.

As in plane flows, the motion around a closed body of revolution can be generated by superposition of a uniform stream and a collection of sources and sinks whose net strength is zero. The closed surface becomes *streamlined* (that is, has a gradually tapering tail) if, for example, the sinks are *distributed* over a finite length. Consider Figure 6.28, where there is a point source Q (m^3/s) at the origin O, and a continuously distributed line sink on the z-axis from O to A (distance $= a$). Let the volume absorbed per unit length of the line sink

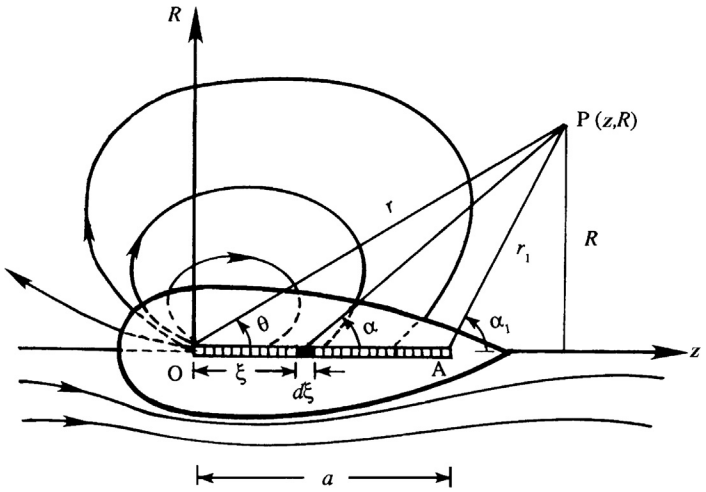

FIGURE 6.28 Ideal flow past an axisymmetric streamlined body generated by a point source at O and a distributed line sink from O to A. The upper half of the figure shows the streamlines induced by the source and the line-segment sink alone. The lower half of the figure shows streamlines when a uniform stream along the axis of symmetry is added to the flow in the upper half of the figure.

be k (m^3/s per m). An elemental length $d\xi$ of the sink can be regarded as a point sink of strength $kd\xi$, for which the stream function at any point P is

$$d\psi_{sink} = \frac{k\,d\xi}{4\pi}\cos\alpha$$

[see (6.87)]. The total stream function at P due to the entire line sink from O to A is

$$\psi_{sink} = \frac{k}{4\pi}\int_0^a \cos\alpha\, d\xi. \tag{6.93}$$

The integral can be evaluated by noting that $z - \xi = R\cot\alpha$. This gives $d\xi = Rd\alpha/\sin^2\alpha$ because z and R remain constant as we go along the sink. The stream function of the line sink is therefore

$$\psi_{sink} = \frac{k}{4\pi}\int_\theta^{\alpha_1} \cos\alpha\frac{R}{\sin^2\alpha}d\alpha = \frac{kR}{4\pi}\int_\theta^{\alpha_1}\frac{d(\sin\alpha)}{\sin^2\alpha}, = \frac{kR}{4\pi}\left[\frac{1}{\sin\theta} - \frac{1}{\sin\alpha_1}\right] = \frac{k}{4\pi}(r - r_1). \tag{6.94}$$

To obtain a closed body, we must adjust the strengths so that the volume flow from the source (Q) is absorbed by the sink, that is, $Q = ak$. Then the stream function at any point P due to the superposition of a point source of strength Q, a distributed line sink of strength $k = Q/a$, and a uniform stream of velocity U along the z-axis, is

$$\psi = -\frac{Q}{4\pi}\cos\theta + \frac{Q}{4\pi a}(r - r_1) + \frac{1}{2}Ur^2\sin^2\theta. \tag{6.95}$$

A plot of the steady streamline pattern is shown in the bottom half of Figure 6.28, in which the top half shows instantaneous streamlines in a frame of reference at rest with respect to the fluid at infinity.

Here we have assumed that the strength of the line sink is uniform along its length. Other interesting streamline patterns can be generated by assuming that the strength $k(\xi)$ is nonuniform.

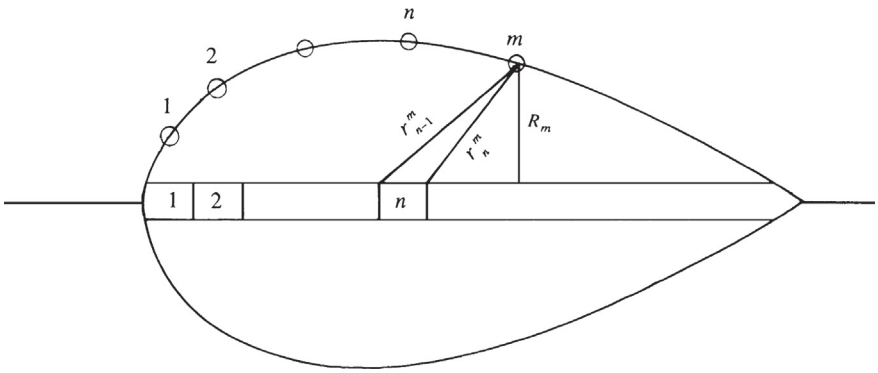

FIGURE 6.29 Flow around an arbitrary axisymmetric shape generated by superposition of a series of line-segment sources distributed along the axis of symmetry.

So far, we have assumed certain distributions of singularities, and then determined the resulting body shape when the distribution is superposed on a uniform stream. The flow around a body with a given shape can be simulated by superposing a uniform stream on a series of sources and sinks of unknown strength distributed on a line coinciding with the axis of the body. The strengths of the sources and sinks are then adjusted so that, when combined with a given uniform flow, a closed stream surface coincides with the given body. Such a calculation is typically done numerically using a computer.

Let the body length L be divided into N equal segments of length $\Delta\xi$, and let k_n be the strength (m^2/s) of one of these line segments, which may be positive or negative (Figure 6.29). The stream function at any body surface point m due to the line-segment source n is, using (6.94),

$$\psi_{mn} = -\frac{k_n}{4\pi}\left(r^m_{n-1} - r^m_n\right),$$

where the negative sign is introduced because (6.94) is for a sink. When combined with a uniform stream, the stream function at point m in Figure 6.29 due to all N line sources is

$$\psi_m = -\sum_{n=1}^{N} \frac{k_n}{4\pi}\left(r^m_{n-1} - r^m_n\right) + \tfrac{1}{2}U R^2_m.$$

Setting $\psi_m = 0$ for all N values of m, we obtain a set of N linear algebraic equations in N unknowns $k_n (n = 1, 2, \ldots, N)$, which can be solved by the iteration technique described in Section 6.7 or a matrix inversion routine.

6.9. THREE-DIMENSIONAL POTENTIAL FLOW AND APPARENT MASS

In three dimensions, ideal flow concepts can be used effectively for a variety of problems in aerodynamics and hydrodynamics. However, d'Alembert's paradox persists and it can be shown that steady ideal flow in three dimensions cannot predict fluid mechanical drag on

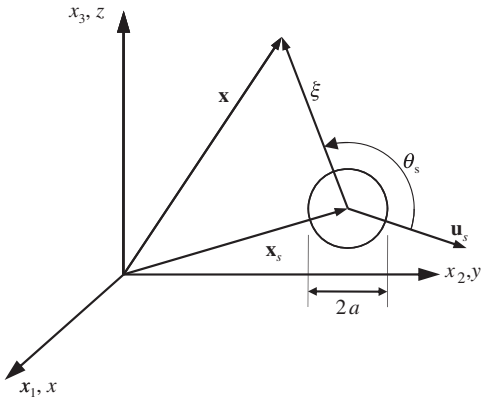

FIGURE 6.30 Three-dimensional geometry for calculating the fluid dynamic force on an arbitrarily moving submerged sphere of radius a centered at $\mathbf{x}_s$. The angle between the sphere's velocity, $\mathbf{u}_s$, and the observation point $\mathbf{x}$ is θ_s. The distance from the center of the sphere to the observation point is ξ.

closed bodies (Exercise 6.39). However, nonzero drag forces can be predicted on submerged three-dimensional objects when the flow is unsteady or some vorticity is present. This section concentrates on the former while leaving the latter to Chapter 14. The objective here is to establish the origin of the *apparent mass* or *added mass* of an accelerating object immersed in a fluid. In general terms, apparent mass is the enhanced and/or altered inertia of an object that is caused by motion of the fluid around the object. Knowledge of apparent mass is essential for predicting the performance of underwater vehicles, lighter-than-air airships, and ultra-light aircraft. It is important for describing and understanding the maneuverability of fish, the dynamics of kites and bubbles, and the differences between sailboat and motorboat motions on the surface of a wavy sea. However, to minimize complexity and to emphasize the core concepts, the focus here is on the simplest possible three-dimensional object, a sphere.

In general, the velocity potential ϕ is extended to the three dimensions merely by considering all three components of its definition $\mathbf{u} \equiv \nabla\phi$ to be nonzero. In Cartesian coordinates, this means augmenting (6.10) to include $w \equiv \partial\phi/\partial z$, where (in this section) w is the z-component of the fluid velocity and z is the third spatial coordinate.

The situation of interest is depicted in Figure 6.30, where a sphere with radius a moves in a quiescent fluid with undisturbed pressure p_∞ via an external force, $\mathbf{F}_E$, that acts only on the sphere.[2] The location $\mathbf{x}_s(t)$, velocity $\mathbf{u}_s(t) = d\mathbf{x}_s/dt$, and acceleration $d\mathbf{u}_s/dt$ of the sphere are presumed known, and the fluid dynamic force $\mathbf{F}_s$ on the sphere is to be determined. This is an idealization of the situation for a maneuvering fish, submarine, or airship.

The potential for an arbitrarily moving sphere is a modified version of (6.92) with the sphere centered at $\mathbf{x}_s(t)$ and the fluid far from the sphere at rest. These changes are implemented by replacing $\mathbf{x}$ in (6.92) with $\mathbf{x} - \mathbf{x}_s(t)$, and by setting $\mathbf{U} = 0$, which leaves:

$$\phi = -\frac{1}{4\pi|\mathbf{x} - \mathbf{x}_s(t)|^3}\mathbf{d}\cdot(\mathbf{x} - \mathbf{x}_s(t)). \tag{6.96}$$

[2]The development provided here is based on a lecture given by Professor P. Dimotakis in 1984.

For this potential to represent a constant-size moving sphere at each instant in time, the dipole strength must continuously change direction and strength to point into the flow impinging on the sphere. If the sphere's velocity is $\mathbf{u}_s(t)$, then, to an observer on the sphere, the oncoming flow velocity is $-\mathbf{u}_s(t)$. Thus, at any instant in time the dipole strength must be $\mathbf{d}(t) = -2\pi a^3[-\mathbf{u}_s(t)]$, a direct extension of the steady flow result. Substitution of this $\mathbf{d}(t)$ into (6.96) produces:

$$\phi(\mathbf{x}, \mathbf{x}_s, \mathbf{u}_s) = -\frac{a^3}{2|\mathbf{x} - \mathbf{x}_s|^3}\mathbf{u}_s \cdot (\mathbf{x} - \mathbf{x}_s) = -\frac{a^3}{2|\boldsymbol{\xi}|^3}\mathbf{u}_s \cdot \boldsymbol{\xi}. \tag{6.97}$$

Here, explicit listing of the time argument of $\mathbf{x}_s$ and $\mathbf{u}_s$ has been dropped for clarity, and $\boldsymbol{\xi} = \mathbf{x} - \mathbf{x}_s$ is the vector distance from the center of the sphere to the location $\mathbf{x}$.

For ideal flow, an integral of the pressure forces over the surface of the sphere determines $\mathbf{F}_s$:

$$\mathrm{F}_s = -\int_{\text{sphere's surface}} (p - p_\infty)\mathbf{n}dA. \tag{6.98}$$

This is the three-dimensional equivalent of (6.55) since $\int p_\infty \mathbf{n}dA = 0$ for a closed surface and constant p_∞. The pressure difference in (6.98) can be obtained from the unsteady Bernoulli equation evaluated on the sphere's surface and far from the sphere where the pressure is p_∞, $\mathbf{u} = 0$, and $\partial\phi/\partial t = 0$:

$$\left[\frac{\partial\phi}{\partial t} + \frac{1}{2}|\nabla\phi|^2 + \frac{p}{\rho}\right]_{\text{sphere's surface}} = \frac{p_\infty}{\rho}. \tag{6.99}$$

For the geometry shown in Figure 6.30 the sphere's surface is defined by $|\mathbf{x} - \mathbf{x}_s| = |\boldsymbol{\xi}| = a$, so for notational convenience the subscript "a" will denote quantities evaluated on the sphere's surface. Thus, (6.99) can be rewritten:

$$\frac{p_a - p_\infty}{\rho} = -\left(\frac{\partial\phi}{\partial t}\right)_a - \frac{1}{2}|\nabla\phi|_a^2. \tag{6.100}$$

The time derivative of ϕ can be evaluated as follows:

$$\frac{\partial}{\partial t}\phi(\mathbf{x}, \mathbf{x}_s, \mathbf{u}_s) = \frac{\partial\phi}{\partial(x_s)_i}\frac{d(x_s)_i}{dt} + \frac{\partial\phi}{\partial(u_s)_i}\frac{d(u_s)_i}{dt} = -\mathbf{u} \cdot \mathbf{u}_s - \frac{a^3}{2|\boldsymbol{\xi}|^3}\boldsymbol{\xi} \cdot \frac{d\mathbf{u}_s}{dt}, \tag{6.101}$$

where the middle of this extended equality presents a temporary switch to index notation. The final form in (6.101) is obtained from the definition $d(x_s)_i/dt = \mathbf{u}_s$, and the fact that $\partial\phi/\partial(x_s)_i = -\partial\phi/\partial x_i = -\mathbf{u}$ for the potential (6.97) since it only depends on $\mathbf{x} - \mathbf{x}_s$. When evaluated on the sphere's surface, this becomes:

$$\left(\frac{\partial\phi}{\partial t}\right)_a = -\mathbf{u}_a \cdot \mathbf{u}_s - \frac{a}{2}\mathbf{e}_\xi \cdot \frac{d\mathbf{u}_s}{dt}, \tag{6.102}$$

where $\mathbf{e}_\xi = \boldsymbol{\xi}/|\boldsymbol{\xi}|$. The independent spatial variable $\mathbf{x}$ appears twice in (6.97) so the gradient of ϕ involves two terms,

$$\nabla\phi \;=\; -\frac{a^3}{2}\left[\,-\frac{3(\mathbf{x}-\mathbf{x}_s)}{|\mathbf{x}-\mathbf{x}_s|^5}\mathbf{u}_s\cdot(\mathbf{x}-\mathbf{x}_s)+\frac{1}{|\mathbf{x}-\mathbf{x}_s|^3}\mathbf{u}_s\right], \tag{6.103}$$

which are readily evaluated on the surface of the sphere where $(\mathbf{x}-\mathbf{x}_s)_a = a\mathbf{e}_\xi$:

$$\mathbf{u}_a \;=\; (\nabla\phi)_a = \;-\frac{a^3}{2}\left[\,-\frac{3a\mathbf{e}_\xi}{a^5}\mathbf{u}_s\cdot a\mathbf{e}_\xi-\frac{1}{a^3}\mathbf{u}_s\right] = \frac{3}{2}\big(\mathbf{u}_s\cdot\mathbf{e}_\xi\big)\;\mathbf{e}_\xi-\frac{1}{2}\mathbf{u}_s. \tag{6.104}$$

Combining (6.100), (6.102), and (6.104) produces a final relationship for the surface pressure p_a on the sphere in terms of the orientation $\mathbf{e}_\xi$, and the sphere's velocity $\mathbf{u}_s$ and acceleration $d\mathbf{u}_s/dt$:

$$\begin{aligned}\frac{p_a-p_\infty}{\rho} \;&=\; \left(\frac{3}{2}\big(\mathbf{u}_s\cdot\mathbf{e}_\xi\big)\;\mathbf{e}_\xi-\frac{1}{2}\mathbf{u}_s\right)\cdot\mathbf{u}_s+\frac{a}{2}\mathbf{e}_\xi\cdot\frac{d\mathbf{u}_s}{dt}-\frac{1}{2}\left|\frac{3}{2}(\mathbf{u}_s\cdot\mathbf{e}_\xi)\;\mathbf{e}_\xi-\frac{1}{2}\mathbf{u}_s\right|^2\\ &=\; \left(\frac{3}{2}\big(\mathbf{u}_s\cdot\mathbf{e}_\xi\big)^2-\frac{1}{2}|\mathbf{u}_s|^2\right)+\frac{a}{2}\mathbf{e}_\xi\cdot\frac{d\mathbf{u}_s}{dt}-\frac{1}{8}\Big(9\big(\mathbf{u}_s\cdot\mathbf{e}_\xi\big)^2-6\big(\mathbf{u}_s\cdot\mathbf{e}_\xi\big)^2+|\mathbf{u}_s|^2\Big)\\ &=\; \frac{1}{2}|\mathbf{u}_s|^2\left(\frac{9}{4}\frac{\big(\mathbf{u}_s\cdot\mathbf{e}_\xi\big)^2}{|\mathbf{u}_s|^2}-\frac{5}{4}\right)+\frac{a}{2}\mathbf{e}_\xi\cdot\frac{d\mathbf{u}_s}{dt}\end{aligned} \tag{6.105}$$

When the sphere is not accelerating and θ_s is the angle between $\mathbf{e}_\xi$ and $\mathbf{u}_s$, then

$$\left(\frac{p_a-p_\infty}{\frac{1}{2}\rho|\mathbf{u}_s|^2}\right)_{steady} \;=\; \frac{9}{4}\cos^2\theta_s-\frac{5}{4} \;=\; 1-\frac{9}{4}\sin^2\theta_s, \tag{6.106}$$

which is identical to (6.91). Thus, as expected from the Galilean invariance of Newtonian mechanics, steady flow past a stationary sphere and steady motion of a sphere through an otherwise quiescent fluid lead to the same pressure distribution on the sphere. And, once again, no drag on the sphere is predicted.

However, (6.105) includes a second term that depends on the direction and magnitude of the sphere's acceleration. To understand the effects of this term, reorient the coordinate system in Figure 6.30 so that at the time of interest the sphere is at the origin of coordinates and its acceleration is parallel to the polar z- or x_3-axis: $d\mathbf{u}_s/dt = |d\mathbf{u}_s/dt|\mathbf{e}_z$. With this revised geometry, $\mathbf{e}_\xi\cdot d\mathbf{u}_s/dt = |d\mathbf{u}_s/dt|\;\cos\theta$, and the fluid dynamic force on the sphere can be obtained from (6.98) in spherical polar coordinates:

$$\mathbf{F}_s \;=\; -\rho\frac{a}{2}\left|\frac{d\mathbf{u}_s}{dt}\right|\int_{\theta=0}^{\pi}\int_{\varphi=0}^{2\pi}\cos\theta\big(\mathbf{e}_x\sin\theta\cos\varphi+\mathbf{e}_y\sin\theta\sin\varphi+\mathbf{e}_z\cos\theta\big)a^2\sin\theta d\varphi d\,\theta. \tag{6.107}$$

The φ-integration causes the x- and y-force components to be zero, leaving:

$$\mathbf{F}_s \;=\; -\pi\rho a^3\left|\frac{d\mathbf{u}_s}{dt}\right|\mathbf{e}_z\int_{\theta=0}^{\pi}\cos^2\theta\;\sin\theta d\varphi d\theta \;=\; -\frac{2}{3}\pi\rho a^3\frac{d\mathbf{u}_s}{dt} \;=\; -M\frac{d\mathbf{u}_s}{dt}, \tag{6.108}$$

where $M = 2\pi a^3\rho/3$ is the *apparent* or *added mass* of the sphere. Thus, the ideal-flow fluid-dynamic force on an accelerating sphere opposes the acceleration, and its magnitude is proportional to the sphere's acceleration and one-half of the mass of the fluid displaced by the sphere.

This fluid-inertia-based loading is the apparent mass or added mass of the sphere. It occurs because fluid must move more rapidly out of the way, in front of, and more rapidly fill in behind, an accelerating sphere. To illustrate its influence, consider an elementary dynamics problem involving a rigid sphere of mass m and radius a that is subject to an external force $\mathbf{F}_E$ while submerged in a large bath of nominally quiescent inviscid fluid with density ρ. In this case, Newton's second law (sum of forces = mass $\times$ acceleration) implies:

$$\mathbf{F}_E + \mathbf{F}_s = \mathbf{F}_E - M\frac{d\mathbf{u}_s}{dt} = m\frac{d\mathbf{u}_s}{dt}, \text{ or } \mathbf{F}_E = \left(m + \frac{2\pi}{3}\rho a^3\right)\frac{d\mathbf{u}_s}{dt}. \tag{6.109}$$

Thus, a submerged sphere will behave as if its inertia is larger by one-half of the mass of the fluid it displaces compared to its behavior in vacuum. For a sphere, the apparent mass is a scalar because of its rotational symmetry. In general, apparent mass is a tensor and the final equality in (6.108) is properly stated $(F_s)_i = M_{ij}\, d(u_s)_j/dt$.

6.10. CONCLUDING REMARKS

The theory of irrotational constant-density (ideal) flow has reached a highly developed stage during the last 250 years because of the efforts of theoretical physicists such as Euler, Bernoulli, d'Alembert, Lagrange, Stokes, Helmholtz, Kirchhoff, and Kelvin. The special interest in the subject has resulted from the applicability of potential theory to other fields such as heat conduction, elasticity, and electromagnetism. When applied to fluid flows, however, the theory predicts zero fluid dynamic drag on a moving body, a result that is at variance with observations. Meanwhile, the theory of viscous flow was developed during the middle of the nineteenth century, after the Navier-Stokes equations were formulated. The viscous solutions generally applied either to very slow flows where the nonlinear advection terms in the equations of motion were negligible, or to flows in which the advective terms were identically zero (such as the viscous flow through a straight pipe). The viscous solutions were highly rotational, and it was not clear where the irrotational flow theory was applicable and why. This was left for Prandtl to explain (see Chapter 9).

It is probably fair to say that ideal flow theory does not occupy center stage in fluid mechanics any longer, although it did so in the past. However, the subject is still quite useful in several fields, especially in aerodynamics and hydrodynamics. We shall see in Chapter 9 that the pressure distribution around streamlined bodies can still be predicted with a fair degree of accuracy from the ideal flow theory. In Chapter 14 we shall see that the lift of an airfoil is due to the development of circulation around it, and the magnitude of the lift agrees with the Kutta-Zhukhovsky lift theorem. The technique of conformal mapping will also be useful in our study of flow around airfoil shapes.

EXERCISES

6.1. **a)** Show that (6.7) solves (6.5) and leads to $\mathbf{u} = (U,V)$.
b) Integrate (6.6) within a circular area centered on (x′, y′) of radius $r' = \sqrt{(x-x')^2+(y-y')^2}$ to show that (6.8) is a solution of (6.6).

6.2. For two-dimensional ideal flow, show separately that:
a) $\nabla\psi\cdot\nabla\phi = 0$
b) $-\nabla\psi\times\nabla\phi = |\mathbf{u}|^2\mathbf{e}_z$
c) $|\nabla\psi|^2 = |\nabla\phi|^2$
d) $\nabla\phi = -\mathbf{e}_z\times\nabla\psi$

6.3. **a)** Show that (6.14) solves (6.12) and leads to $\mathbf{u} = (U,V)$.
b) Integrate (6.13) within circular area centered on (x', y') of radius $r' = \sqrt{(x-x')^2+(y-y')^2}$ to show that (6.15) is a solution of (6.13).
c) For the flow described by (6.15), show that the volume flux (per unit depth into the page) $= \oint_C \mathbf{u}\cdot\mathbf{n}ds$ computed from a closed contour C that encircles the point (x', y') is m. Here $\mathbf{n}$ is the outward normal on C and ds is a differential element of C.

6.4. Show that (6.1) reduces to $\frac{\partial\phi}{\partial t} + \frac{1}{2}|\nabla\phi|^2 + \frac{p}{\rho} = const.$ when the flow is described by the velocity potential ϕ.

6.5. Determine u and v, and sketch streamlines for:
a) $\psi = A(x^2 - y^2)$
b) $\phi = A(x^2 - y^2)$

6.6. Assume $\psi = ax^3 + bx^2y + cxy^2 + dy^3$ where a, b, c, and d are constants; and determine two independent solutions to the Laplace equation. Sketch the streamlines for both flow fields.

6.7. Repeat Exercise 6.6 for $\psi = ax^4 + bx^3y + cx^2y^2 + dxy^3 + ey^4$ where a, b, c, d, and e are constants.

6.8. Without using complex variables, determine:
a) The potential ϕ for an ideal vortex of strength Γ starting from (6.8).
b) The stream function for an ideal point source of strength Q starting from (6.15).
c) Is there any ambiguity in your answers to parts a) and b)? If so, does this ambiguity influence the fluid velocity?

6.9. Determine the stream function of a doublet starting from (6.29) and show that the streamlines are circles having centers on the y-axis that are tangent to the x-axis at the origin.

6.10. Consider steady horizontal flow at speed U past a stationary source of strength m located at the origin of coordinates in two dimensions, (6.30) or (6.31). To hold it in place, an external force per unit depth into the page, $\mathbf{F}$, is applied to the source.
a) Develop a dimensionless scaling law for $F = |\mathbf{F}|$.
b) Use a cylindrical control volume centered on the source with radius R and having depth B into the page, the steady ideal-flow momentum conservation equation for a control volume,

$$\int_{A^*} \rho\mathbf{u}(\mathbf{u}\cdot\mathbf{n})dA = -\int_{A^*} p\mathbf{n}dA + \mathrm{F},$$

and an appropriate Bernoulli equation to determine the magnitude and direction of $\mathbf{F}$.

c) Is the direction of **F** unusual in any way? Explain it physically.

6.11. Repeat all three parts of Exercise 6.10 for steady ideal flow past a stationary irrotational vortex located at the origin when the control volume is centered on the vortex. The stream function for this flow is: $\psi = Ur\sin\theta - (\Gamma/2\pi)\ln(r)$.

6.12. Use the principle of conservation of mass (4.5) and an appropriate control volume to show that maximum half thickness of the half-body described by (6.30) or (6.31) is $h_{max} = m/2U$.

6.13. By integrating the surface pressure, show that the drag on a plane half-body (Figure 6.7) is zero.

6.14. Ideal flow past a cylinder (6.33) is perturbed by adding a small vertical velocity without changing the orientation of the doublet:

$$\psi = -U\gamma x + Uy - \frac{Ua^2y}{x^2+y^2} = -U\gamma r\cos\theta + U\left(r - \frac{a^2}{r}\right)\sin\theta.$$

a) Show that the stagnation point locations are $r_s = a$ and $\theta_s = \gamma/2, \pi + \gamma/2$ when $\gamma \ll 1$.

b) Does this flow include a closed body?

6.15. For the following flow fields (b, U, Q, and Γ are positive real constants), sketch streamlines.

a) $\psi = b\sqrt{r}\cos(\theta/2)$ for $|\theta| < 180^\circ$

b) $\psi = Uy + (\Gamma/2\pi)\left[\ln(\sqrt{x^2+(y-b)^2}) - \ln(\sqrt{x^2+(y+b)^2})\right]$

c) $\phi = \sum_{n=-\infty}^{n=+\infty}(Q/2\pi)\ln\left(\sqrt{x^2+(y-2na)^2}\right)$ for $|y| < a$

6.16. [1]Take a standard sheet of paper and cut it in half. Make a simple airfoil with one half and a cylinder with the other half that are approximately the same size as shown.

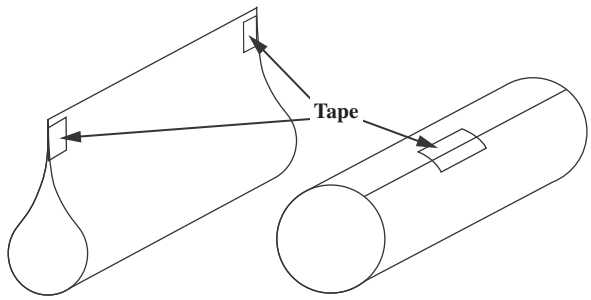

a) If the cylinder and the airfoil are dropped from the same height at the same time with the airfoil pointed toward the ground in its most streamlined configuration, predict which one reaches the ground first.

b) Stand on a chair and perform this experiment. What happens? Are your results repeatable?

c) Can you explain what you observe?

[1]Based on a suggestion from Professor William Schultz

6.17. Consider the following two-dimensional stream function composed of a uniform horizontal stream of speed U and two vortices of equal and opposite strength in (x,y)-Cartesian coordinates.

$$\psi(x,y) = Uy + (\Gamma/2\pi)\ln\sqrt{x^2+(y-b)^2} - (\Gamma/2\pi)\ln\sqrt{x^2+(y+b)^2}$$

a) Simplify this stream function for the combined limit of $b\to 0$ and $\Gamma\to\infty$ when $2b\Gamma = C =$ constant to find: $\psi(x,y) = Uy(1-(C/2\pi U)(x^2+y^2)^{-1})$.
b) Switch to (r,θ)-polar coordinates and find both components of the velocity using the simplified stream function.
c) For the simplified stream function, determine where $u_r = 0$.
d) Sketch the streamlines for the simplified stream function, and describe this flow.

6.18. Graphically generate the streamline pattern for a plane half-body in the following manner. Take a source of strength $m = 200\ \text{m}^2/\text{s}$ and a uniform stream $U = 10\ \text{m/s}$. Draw radial streamlines from the source at equal intervals of $\Delta\theta = \pi/10$, with the corresponding stream function interval

$$\Delta\psi_{\text{source}} = \frac{m}{2\pi}\Delta\theta = 10\ \text{m}^2/\text{s}.$$

Now draw streamlines of the uniform flow with the same interval, that is,

$$\Delta\psi_{\text{stream}} = U\,\Delta y = 10\ \text{m}^2/\text{s}.$$

This requires $\Delta y = 1$ m, which you can plot assuming a linear scale of 1 cm = 1 m. Now connect points of equal $\psi = \psi_{\text{source}} + \psi_{\text{stream}}$.

6.19. Consider the two-dimensional steady flow formed by combining a uniform stream of speed U in the positive x direction, a source of strength $m > 0$ at $(x,y) = (-a,0)$, and a sink of strength m at $(x,y) = (+a,0)$ where $a > 0$. The pressure far upstream of the origin is p_∞.
a) Write down the velocity potential and the stream function for this flow field.
b) What are the coordinates of the stagnation points?
c) Determine the pressure in this flow field along the y-axis.

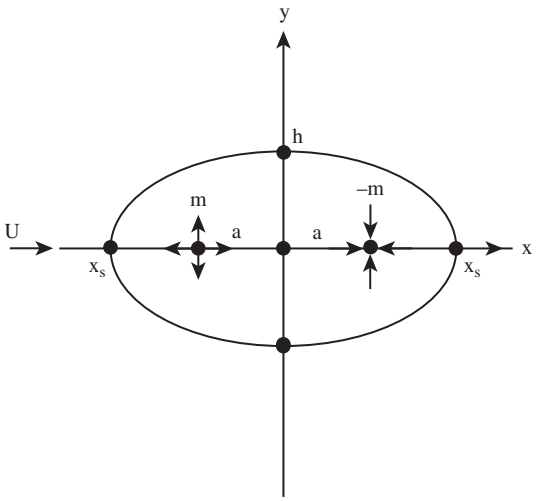

d) There is a closed streamline in this flow that defines a Rankine body. Obtain a transcendental algebraic equation for this streamline, and show that the half-width, h, of the body in the y direction is given by: $\frac{h}{a} = \cot\left(\frac{\pi U h}{m}\right)$. (The introduction of angles may be useful here.)

6.20. A stationary ideal two-dimensional vortex with clockwise circulation Γ is located at point $(0, a)$, above a flat plate. The plate coincides with the x-axis. A uniform stream U directed along the x-axis flows over the vortex. Sketch the flow pattern and show that it represents the flow over an oval-shaped body when $\Gamma/\pi a > U$. [*Hint*: Introduce the image vortex and locate the two stagnation points on the x-axis.]

If the pressure at $x = \pm\infty$ is P_∞, and that *below* the plate is also P_∞, then show that the pressure at any point on the plate is given by: $p_\infty - p = \frac{\rho\Gamma^2 a^2}{2\pi^2(x^2+a^2)^2} - \frac{\rho U\Gamma a}{\pi(x^2+a^2)}$.

Show that the total upward force per unit depth on the plate is: $F = \frac{\rho\Gamma^2}{4\pi a} - \rho U\Gamma$.

6.21. Consider plane flow around a circular cylinder. Use the complex potential and Blasius theorem (6.60) to show that the drag is zero and the lift is $L = \rho U\Gamma$. (In Section 6.3, these results were obtained by integrating the surface pressure distribution.)

6.22. For the doublet flow described by (6.29) and sketched in Figure 6.6, show $u < 0$ for $y < x$ and $u > 0$ for $y > x$. Also, show that $v < 0$ in the first quadrant and $v > 0$ in the second quadrant.

6.23. Hurricane winds blow over a *Quonset hut*, that is, a long half-circular cylindrical cross-section building, 6 m in diameter. If the velocity far upstream is $U_\infty = 40$ m/s and $p_\infty = 1.003 \times 10^5$ N/m, $\rho_\infty = 1.23$ kg/m^3, find the force per unit depth on the building, assuming the pressure inside the hut is a) p_∞, and b) stagnation pressure, $p_\infty + \frac{1}{2}\rho_\infty U_\infty^2$.

6.24. In a two-dimensional ideal flow, a source of strength m is located a meters above an infinite plane. Find the velocity on the plane, the pressure on the plane, and the reaction force on the plane assuming constant pressure p_∞ below the plane.

6.25. Consider a two-dimensional ideal flow over a circular cylinder of radius $r = a$ with axis coincident with a right-angle corner, as shown in the figure below. Assuming that $\psi = Axy$ (with A = constant) when the cylinder is absent, solve for the stream function and velocity components.

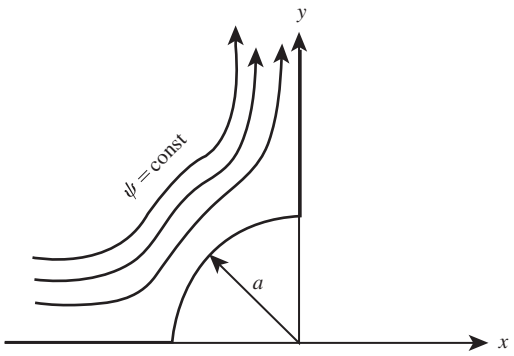

6.26. Consider the following two-dimensional velocity potential consisting of two sources and one sink, all of strength m:

$$\phi(x,y) = (m/2\pi)\left(\ln\sqrt{(x-b)^2+y^2} + \ln\sqrt{(x-a^2/b)^2+y^2} - \ln\sqrt{x^2+y^2}\right).$$

Here a and b are positive constants and $b > a$.

a) Determine the locations of the two stagnation points in this flow field.

b) Sketch the streamlines in this flow field.

c) Show that the closed streamline in this flow is given by $x^2 + y^2 = a^2$ by finding the radial location where $u_r = 0$.

6.27. Without using complex variables, derive the results of the Kutta-Zhukhovsky lift theorem (6.62) for steady two-dimensional irrotational constant-density flow past an arbitrary-cross-section object by considering the *clam-shell* control volume (shown as a dashed line) in the limit as $r \to \infty$. Here A_1 is a large circular contour, A_2 follows the object's cross-section contour, and A_3 connects A_1 and A_2. Let p_∞ and $U\mathbf{e}_x$ be the pressure and flow velocity far from the origin of coordinates, and denote the flow extent perpendicular to the x-y plane by B.

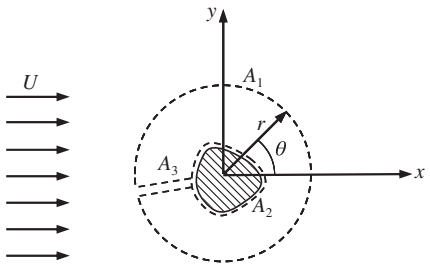

6.28. Pressure fluctuations in wall-bounded turbulent flows are a common source of flow noise. Such fluctuations are caused by turbulent eddies as they move over the bounding surface. A simple ideal-flow model that captures some of the important phenomena involves a two-dimensional vortex that moves above a flat surface in a fluid of density ρ. Thus, for the following items, use the potential:

$$\phi(x,y,t) = -\frac{\Gamma}{2\pi}\tan^{-1}\left(\frac{y-h}{x-Ut}\right) + \frac{\Gamma}{2\pi}\tan^{-1}\left(\frac{y+h}{x-Ut}\right),$$

where h is the distance of the vortex above the flat surface, Γ is the vortex strength, and U is the convection speed of the vortex.

a) Compute the horizontal u and vertical v velocity components and verify that $v = 0$ on $y = 0$.

b) Determine the pressure at $x = y = 0$ in terms of ρ, t, Γ, h, and U.

c) Based on your results from part b), is it possible for a fast-moving, high-strength vortex far from the surface to have the same pressure signature as a slow-moving, low-strength vortex closer to the surface?

6.29. A pair of equal strength ideal line vortices having axes perpendicular to the x-y plane are located at $\mathbf{x}_a(t) = (x_a(t), y_a(t))$, and $\mathbf{x}_b(t) = (x_b(t), y_b(t))$, and move in their mutually induced velocity fields. The stream function for this flow is given by: $\psi(x,y,t) = -\dfrac{\Gamma}{2\pi}(\ln|\mathbf{x} - \mathbf{x}_a(t)| + \ln|\mathbf{x} - \mathbf{x}_b(t)|)$. Explicitly determine $\mathbf{x}_a(t)$ and $\mathbf{x}_b(t)$, given $\mathbf{x}_a(0) = (-r_o, 0)$ and $\mathbf{x}_b(0) = (r_o, 0)$. Switching to polar coordinates at some point in your solution may be useful.

6.30. Consider the unsteady potential flow of two ideal sinks located at $\mathbf{x}_a(t) = (x_a(t), 0)$ and $\mathbf{x}_b(t) = (x_b(t), 0)$ that are free to move along the x-axis in an ideal fluid that is stationary far from the origin. Assume that each sink will move in the velocity field induced by the other.

$$\phi(x,y,t) = -\frac{Q}{2\pi}\left[\ln\sqrt{(x - x_a(t))^2 + y^2} + \ln\sqrt{(x - x_b(t))^2 + y^2}\right], \text{ with } Q > 0.$$

a) Determine $x_a(t)$ and $x_b(t)$ when $\mathbf{x}_a(0) = (-L, 0)$ and $\mathbf{x}_b(0) = (+L, 0)$.
b) If the pressure far from the origin is p_∞ and the fluid density is ρ, determine the pressure p at $x = y = 0$ as a function of p_∞, ρ, Q, and $x_a(t)$.

6.31. Consider the unsteady potential flow of an ideal source and sink located at $\mathbf{x}_1(t) = (x_1(t), 0)$ and $\mathbf{x}_2(t) = (x_2(t), 0)$ that are free to move along the x-axis in an ideal fluid that is stationary far from the origin. Assume that the source and sink will move in the velocity field induced by the other.

$$\phi(x,y,t) = \frac{m}{2\pi}\left[\ln\sqrt{(x - x_1(t))^2 + y^2} - \ln\sqrt{(x - x_2(t))^2 + y^2}\right], \text{ with } m > 0.$$

a) Determine $x_1(t)$ and $x_2(t)$ when $\mathbf{x}_1(0) = (-\lambda, 0)$ and $\mathbf{x}_2(0) = (+\lambda, 0)$.
b) If the pressure far from the origin is p_∞ and the fluid density is ρ, determine the pressure p at $x = y = 0$ as a function of p_∞, ρ, m, λ, and t.

6.32. Consider a free ideal line vortex oriented parallel to the z-axis in a 90° corner defined by the solid walls $\theta = 0$ and $\theta = 90°$. If the vortex passes through the plane of the flow at (x, y), show that the vortex path is given by: $\frac{1}{x^2} + \frac{1}{y^2} =$ constant. [*Hint*: Three image vortices are needed at points $(-x, -y)$, $(-x, y)$, and $(x, -y)$. Carefully choose the directions of rotation of these image vortices, show that $dy/dx = v/u = -y^3/x^3$, and integrate to produce the desired result.]

6.33. In ideal flow, streamlines are defined by $d\psi = 0$, and potential lines are defined by $d\phi = 0$. Starting from these relationships, show that streamlines and potential lines are perpendicular:
a) in plane flow where x and y are the independent spatial coordinates, and
b) in axisymmetric flow where R and z are the independent spatial coordinates.
[Hint: For any two independent coordinates x_1 and x_2, the unit tangent to the curve $x_2 = f(x_1)$ is $\mathbf{t} = (\mathbf{e}_1 + (df/dx_1)\mathbf{e}_2)/\sqrt{1 + (df/dx_1)^2}$; thus, for parts a) and b) it is sufficient to show $(\mathbf{t})_{\psi=const} \cdot (\mathbf{t})_{\phi=const} = 0$.]

6.34. Consider a three-dimensional point source of strength Q (m^3/s). Use a spherical control volume and the principle of conservation of mass to argue that the velocity components in spherical coordinates are $u_\theta = 0$ and $u_r = Q/4\pi r^2$ and that the velocity potential and stream function must be of the form $\phi = \phi(r)$ and $\psi = \psi(\theta)$. Integrate the velocity, to show that $\phi = -Q/4\pi r$ and $\psi = -Q\cos\theta/4\pi$.

6.35. Solve the Poisson equation $\nabla^2\phi = Q\delta(\mathbf{x} - \mathbf{x}')$ in a uniform, unbounded three-dimensional domain to obtain the velocity potential $\phi = -Q/4\pi|\mathbf{x} - \mathbf{x}'|$ for an ideal point source located at $\mathbf{x}'$.

6.36. Using (R, φ, z)-cylindrical coordinates, consider steady three-dimensional potential flow for a point source of strength Q at the origin in a free stream flowing along the z-axis at speed U:

$$\phi(R, \varphi, z) = Uz - \frac{Q}{4\pi\sqrt{R^2 + z^2}}.$$

- **a)** Sketch the streamlines for this flow in any R-z half-plane.
- **b)** Find the coordinates of the stagnation point that occurs in this flow.
- **c)** Determine the pressure gradient, ∇p, at the stagnation point found in part b).
- **d)** If $R = a(z)$ defines the stream surface that encloses the fluid that emerges from the source, determine $a(z)$ for $z \to +\infty$.
- **e)** Use Stokes' stream function to determine an equation for $a(z)$ that is valid for any value of z.
- **f)** Use the control-volume momentum equation, $\int_S \rho\mathbf{u}(\mathbf{u}\cdot\mathbf{n})dA = -\int_S p\mathbf{n}dA + \mathbf{F}$ where $\mathbf{n}$ is the outward normal from the control volume, to determine the force $\mathbf{F}$ applied to the point source to hold it stationary.
- **g)** If the fluid expelled from the source is replaced by a solid body having the same shape, what is the drag on the front of this body?

6.37. In (R, φ, z) cylindrical coordinates, the three-dimensional potential for a point source at (0,0,s) is given by: $\phi = -(Q/4\pi)[R^2 + (z - s)^2]^{-1/2}$.

- **a)** By combining a source of strength $+Q$ at (0,0,$-b$), a sink of strength $-Q$ at (0, 0, $+b$), and a uniform stream with velocity $U\mathbf{e}_z$, derive the potential (6.89) for flow around a sphere of radius a by taking the limit as $Q \to \infty$ and $b \to 0$, such that $\mathbf{d} = -2bQ\mathbf{e}_z = -2\pi a^3 U\mathbf{e}_z = \text{constant}$. Put your final answer in spherical coordinates in terms of U, r, θ, and a.
- **b)** Repeat part a) for the Stokes stream function starting from $\psi = -(Q/4\pi)(z - s)[R^2 + (z - s)^2]^{-1/2}$.

6.38.

- **a)** Determine the locus of points in uniform ideal flow past a circular cylinder of radius a without circulation where the velocity perturbation produced by the presence of the cylinder is 1% of the free-stream value.
- **b)** Repeat for uniform ideal flow past a sphere.
- **c)** Explain the physical reason(s) for the differences between the answers for parts a) and b).

6.39. Using the figure for Exercise 6.27 with $A_3 \to 0$ and $r \to \infty$, expand the three-dimensional potential for a stationary arbitrary-shape closed body in inverse powers of the distance r and prove that ideal flow theory predicts zero drag on the body.

6.40. Consider steady ideal flow over a hemisphere of constant radius a lying on the y-z plane. For the spherical coordinate system shown, the potential for this flow is:

$$\phi(r,\theta,\varphi) = Ur\left(1 + a^3/2r^3\right)\cos\theta,$$

where U is the flow velocity far from the hemisphere. Assume gravity acts downward along the x-axis. Ignore fluid viscosity in this problem.

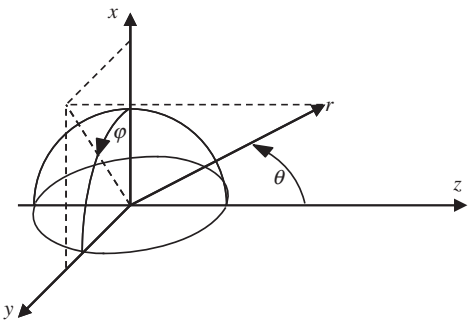

a) Determine all three components of the fluid velocity on the surface of the hemisphere, $r = a$, in spherical polar coordinates: $(u_r, u_\theta, u_\varphi) = \nabla\phi = \left(\frac{\partial\phi}{\partial r}, \frac{1}{r}\frac{\partial\phi}{\partial\theta}, \frac{1}{r\sin\theta}\frac{\partial\phi}{\partial\varphi}\right)$.

b) Determine the pressure, p, on $r = a$.

c) Determine the hydrodynamic force, R_x, on the hemisphere assuming stagnation pressure is felt everywhere underneath the hemisphere. *[Hints*: $\mathbf{e}_r \cdot \mathbf{e}_x = \sin\theta\cos\varphi$, $\int_0^\pi \sin^2\theta d\theta = \pi/2$, and $\int_0^\pi \sin^4\theta d\theta = 3\pi/8$.]

d) For the conditions of part c) what density ρ_h must the hemisphere have to remain on the surface.

6.41. The flow-field produced by suction flow into a round vacuum cleaner nozzle held above a large flat surface can be easily investigated with a simple experiment, and analyzed via potential flow in (R, φ, z)-cylindrical coordinates with the method of images.

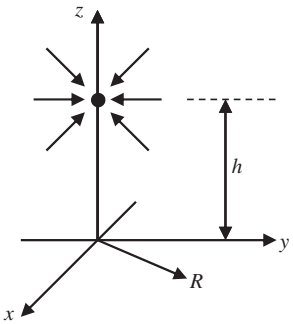

a) Do the experiment first. Obtain a vacuum cleaner that has a hose for attachments. Remove any cleaning attachments (brush, wand, etc.) or unplug the hose from the cleaning head, and attach an extension hose or something with a round opening (~4 cm diameter is recommended). Find a smooth, dry, flat horizontal surface that is a ~0.5 meter or more in diameter. Sprinkle the central third of the surface with a light granular material that is easy to see (granulated sugar, dry coffee grounds, salt, flour, talcum powder, etc., should work well). The grains should be 0.5 to 1 mm apart on average. Turn on the vacuum cleaner and lower the vacuum hose opening from ~0.25 meter above the surface toward the surface with the vacuum opening facing toward the surface. When the hose gets to within about one opening diameter of the surface or so, the granular material should start to move. Once the granular material starts moving, hold the hose opening at the same height or lift the hose slightly so that grains are not sucked into it. If many grains are vacuumed up, distribute new ones in the bare spot(s) and start over. Once the correct hose-opening-to-surface distance is achieved, hold the hose steady and let the suction airflow of the vacuum cleaner scour a pattern into the distributed granular material. Describe the shape of the final pattern, and measure any relevant dimensions.

Now see if ideal flow theory can explain the pattern observed in part a). As a first approximation, the flow field near the hose inlet can be modeled as a sink (a source with strength $-Q$) above an infinite flat boundary since the vacuum cleaner outlet (a source with strength $+Q$) is likely to be far enough away to be ignored. Denote the fluid density by ρ, the pressure far away by p_∞, and the pressure on the flat surface by $p(R)$. The potential for this flow field will be the sum of two terms:

$$\phi(R,z) = \frac{+Q}{4\pi\sqrt{R^2+(z-h)^2}} + K(R,z).$$

b) Sketch the streamlines in the y-z plane for $z > 0$.

c) Determine $K(R,z)$.

d) Use dimensional analysis to determine how $p(R) - p_\infty$ must depend on ρ, Q, R, and h.

e) Compute $p(R) - p_\infty$ from the steady Bernoulli equation. Is this pressure distribution consistent with the results of part a)? Where is the lowest pressure? (This is also the location of the highest speed surface flow.) Is a grain at the origin of coordinates the one most likely to be picked up by the vacuum cleaner?

6.42. There is a point source of strength Q (m^3/s) at the origin, and a uniform line sink of strength $k = Q/a$ extending from $z = 0$ to $z = a$. The two are combined with a uniform stream U parallel to the z-axis. Show that the combination represents the flow past a closed surface of revolution of airship shape, whose total length is the difference of the roots of:

$$\frac{z^2}{a^2}\left(\frac{z}{a} \pm 1\right) = \frac{Q}{4\pi U a^2}.$$

6.43. Using a computer, determine the surface contour of an axisymmetric half-body formed by a line source of strength k (m^2/s) distributed uniformly along the z-axis from $z = 0$

to $z = a$ and a uniform stream. The nose of this body is more pointed than that formed by the combination of a point source and a uniform stream. From a mass balance, show that far downstream the radius of the half-body is $r = \sqrt{ak/\pi U}$.

6.44. [2]Consider the radial flow induced by the collapse of a spherical cavitation bubble of radius $R(t)$ in a large quiescent bath of incompressible inviscid fluid of density ρ. The pressure far from the bubble is p_∞. Ignore gravity.

a) Determine the velocity potential $\phi(r,t)$ for the radial flow outside the bubble.

b) Determine the pressure $p(R(t), t)$ on the surface of the bubble.

c) Suppose that at $t = 0$ the pressure on the surface of the bubble is p_∞, the bubble radius is R_o, and its initial velocity is $-\dot{R}_o$ (i.e., the bubble is shrinking); how long will it take for the bubble to completely collapse if its surface pressure remains constant?

6.45. Derive the apparent mass per unit depth into the page of a cylinder of radius a that travels at speed $U_c(t) = dx_c/dt$ along the x-axis in a large reservoir of an ideal quiescent fluid with density ρ. Use an appropriate Bernoulli equation and the following time-dependent two-dimensional potential: $\phi(x,y,t) = -\dfrac{a^2 U_c(x - x_c)}{(x - x_c)^2 + y^2}$, where $x_c(t)$ is location of the center of the cylinder, and the Cartesian coordinates are x and y. [*Hint*: Steady cylinder motion does *not* contribute to the cylinder's apparent mass; keep only the term (or terms) from the Bernoulli equation necessary to determine apparent mass.]

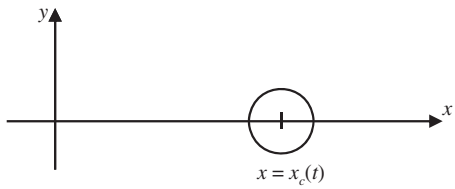

6.46. A stationary sphere of radius a and mass m resides in inviscid fluid with constant density ρ.

a) Determine the buoyancy force on the sphere when gravity g acts downward.

b) At $t = 0$, the sphere is released from rest. What is its initial acceleration?

c) What is the sphere's initial acceleration if it is a bubble in a heavy fluid (i.e., when $m \to 0$)?

6.47. A sphere of mass m and volume V is attached to the end of a light, thin, flexible cable of length L. In a vacuum, with gravity g acting, the natural frequencies for small longitudinal (bouncing) and transverse (pendulum) oscillations of the sphere are ω_b and ω_p. Ignore the effects of viscosity and estimate these natural frequencies when the same sphere and cable are submerged in water with density ρ_w. What is ω_p when $m \ll \rho_w V$?

6.48. Determine the ideal-flow force on a stationary sphere for the following unsteady flow conditions.

[2]Based on problem 5.7 in Currie (1993)

a) The free stream of velocity $U\boldsymbol{e}_z$ is constant but the sphere's radius $a(t)$ varies.
b) The free stream velocity magnitude changes, $U(t)\boldsymbol{e}_z$, but the sphere's radius a is constant.
c) The free stream velocity changes direction $U(\mathbf{e}_x\cos\Omega t + \mathbf{e}_y\sin\Omega t)$, but its magnitude U and the sphere's radius a are constant.

6.49. In three dimensions, consider a solid object moving with velocity $\mathbf{U}$ near the origin of coordinates in an unbounded quiescent bath of inviscid incompressible fluid with density ρ. The kinetic energy of the moving fluid in this situation is:

$$KE = \frac{1}{2}\rho \int_V |\nabla\phi|^2 dV,$$

where ϕ is the velocity potential and V is a control volume that contains all of the moving fluid but excludes the object. (Such a control volume is shown in the figure for Exercise 6.27 when $A_3 \to 0$ and $U = 0$.)

a) Show that $KE = -\frac{1}{2}\rho \int_A \phi(\nabla\phi \cdot \mathbf{n}) dA$ where A encloses the body and is coincident with its surface, and $\mathbf{n}$ is the outward normal on A.
b) The apparent mass, M, of the moving body may be defined by $KE = \frac{1}{2}M|\mathbf{U}|^2$. Using this definition, the result of part a), and (6.97) with $\mathbf{x}_s = 0$, show that $M = 2\pi a^3\rho/3$ for a sphere.

Literature Cited

Carrier, G. F., Krook, M., and Pearson, C. E. (1966). *Functions of a Complex Variable*. New York: McGraw-Hill.
Churchill, R. V., Brown, J. W., and Verhey, R. F. (1974). *Complex Variables and Applications* (3rd ed.). New York: McGraw-Hill.
Currie, I. G. (1993). *Fundamentals of Fluid Mechanics* (2nd ed.). New York: McGraw Hill.
Prandtl, L. (1952). *Essentials of Fluid Dynamics*. New York: Hafner Publishing.

Supplemental Reading

Batchelor, G. K. (1967). *An Introduction to Fluid Dynamics*. London: Cambridge University Press.
Milne-Thompson, L. M. (1962). *Theoretical Hydrodynamics*. London: Macmillan Press.
Shames, I. H. (1962). *Mechanics of Fluids*. New York: McGraw-Hill.
Vallentine, H. R. (1967). *Applied Hydrodynamics*. New York: Plenum Press.